J. Fluid Mech. (2018), *vol.* 844, *pp.* 567–596. © Cambridge University Press 2018
doi:10.1017/jfm.2018.170

Deformation of an encapsulated bubble in steady and oscillatory electric fields

Yunqiao Liu[1], Dongdong He[2], Xiaobo Gong[1,†] and Huaxiong Huang[3,4]

[1]Key Laboratory of Hydrodynamics (Ministry of Education), Department of Engineering Mechanics, Shanghai Jiao Tong University, Shanghai 200240, China

[2]School of Science and Engineering, The Chinese University of Hong Kong, Shenzhen, Guangdong 518172, China

[3]Department of Mathematics and Statistics, York University, Toronto, Ontario M3J 1P3, Canada

[4]The Fields Institute for Research in Mathematical Sciences, Toronto, Ontario M5T 3J1, Canada

(Received 28 August 2017; revised 8 February 2018; accepted 13 February 2018; first published online 6 April 2018)

In this paper, we investigate the dynamics of an encapsulated bubble in steady and oscillatory electric fields theoretically, based on a leaky dielectric model. On the bubble surface, an applied electric field generates a Maxwell stress, in addition to hydrodynamic traction and membrane mechanical stress. Our model also includes the effect of interfacial charge due to the jump of the current and the stretching of the interface. We focus on the axisymmetric deformation of the encapsulated bubble induced by the electric field and carry out our analysis using Legendre polynomials. In our first example, the encapsulating membrane is modelled as a nearly incompressible interface with bending rigidity. Under a steady uniform electric field, the encapsulated bubble resumes an elongated equilibrium shape, dominated by the second- and fourth-order shape modes. The deformed shape agrees well with experimental observations reported in the literature. Our model reveals that the interfacial charge distribution is determined by the magnitude of the shape modes, as well as the permittivity and conductivity of the external and internal fluids. The effects of the electric field on the natural frequency of the oscillating bubble are also shown. For our second example, we considered a bubble encapsulated with a hyperelastic membrane with bending rigidity, subject to an oscillatory electric field. We show that the bubble can modulate its oscillating frequency and reach a stable shape oscillation at an appreciable amplitude.

Key words: bubble dynamics, electrohydrodynamic effects, membranes

1. Introduction

Encapsulated bubbles are widely used in various biomedical applications, e.g. as contrast enhancing agents in ultrasound imaging (Lindner 2004) and as carriers in drug delivery systems (Unger *et al.* 2001). In both cases, controlling the residence time is important. As contrast agents, resonance of bubbles with the applied ultrasound

† Email address for correspondence: x.gong@sjtu.edu.cn

https://doi.org/10.1017/jfm.2018.170 Published online by Cambridge University Press

field is not desirable, since it reduces the residence time. As drug delivery carriers, on the other hand, resonance is used for breaking up the bubbles and increasing drug delivery efficiency. Therefore, it is important to understand the dynamics of encapsulated bubbles subject to applied physical forces, and a key set of parameters are their natural frequencies.

In principle, the natural frequencies of encapsulated bubbles are determined by the flow conditions and the mechanical properties of the membrane. The properties of membranes, such as elastic modulus and bending rigidity, can be measured using micropipette aspiration, atomic force microscopy, optical tweezers (Van Vliet, Bao & Suresh 2003) or the features of fluid flows (Chang & Olbricht 1993*a*,*b*; Lefebvre *et al.* 2008; Knoche *et al.* 2013; De Loubens *et al.* 2015, 2016). These approaches to measuring membrane properties are applicable to vesicles or capsules, but not to encapsulated bubbles, since the latter tend to burst during experiments. The elastic modulus and viscosity of the coating membranes for bubbles were inferred through observing radial pulsation (De Jong *et al.* 2009; Tu *et al.* 2009; Segers *et al.* 2016) and combining constitutive models (Church 1995; Chatterjee & Sarkar 2003; Marmottant *et al.* 2005). However, measurements and models based on radial oscillations cannot be extended to shape oscillations directly. The deformation and collapse of the encapsulated bubbles are related to more complicated mechanical characteristics (Stride & Saffari 2003; Pu, Borden & Longo 2006). For example, microscopic folds contribute to the stabilization of coated membranes, probably because bending rigidity dominates (Kwan & Borden 2012).

Ultrasound provides an approach for estimating the natural frequencies of encapsulated bubbles, bypassing specific mechanical parameters and constitutive laws. The main natural frequency can be estimated from resonance in the radial oscillation patterns by modulating the ultrasonic frequency (van der Meer *et al.* 2007). However, knowing the main radial natural frequency is not sufficient, since the natural frequencies of shape modes are crucial for controlling membrane stability. Using ultrasound to estimate the natural frequencies of shape oscillation is non-trivial due to the fact that the shape modes of a bubble are indirectly related to the ultrasound field (induced by parametric instability of the radial oscillation (Plesset & Prosperetti 1977; Feng & Leal 1997; Brenner, Hilgenfeldt & Lohse 2002)), unlike radial oscillation, which is directly driven by the ultrasound field. Therefore, an alternative approach capable of controlling shape oscillation and estimating natural frequencies of the shape modes directly is needed.

A number of studies have shown that a uniform electric field can be used to induce deformations of gas bubbles (Lee & Kang 1999; Dong *et al.* 2006; Spelt & Matar 2006; Shaw, Spelt & Matar 2009), drops (Taylor 1964; Kang 1993; Trinh, Holt & Thiessen 1996; Dubash & Mestel 2007) and vesicles (Kummrow & Helfrich 1991; Vlahovska *et al.* 2009; Schwalbe, Vlahovska & Miksis 2011). Electro-deformation is utilized to measure membrane properties such as viscosity and bending rigidity (Kummrow & Helfrich 1991; Gracià *et al.* 2010; Salipante & Vlahovska 2014). In this paper, we show that applying an oscillatory electric field offers another non-invasive way for estimating natural frequencies of shape modes when an encapsulated bubble undergoes oscillations.

Although the dynamics of encapsulated bubbles in an ultrasound field has been widely investigated (Ferrara, Pollard & Borden 2007; Stride & Coussios 2010; Lacour *et al.* 2018), not much work has been done on the encapsulated bubble in an oscillating electric field, perhaps due to the increased complexity involving bubble dynamics, electrodynamics and membrane mechanics. The ultrasound field

https://doi.org/10.1017/jfm.2018.170 Published online by Cambridge University Press

could be simply modelled as a pressure wave. By contrast, modelling the dynamics of encapsulated bubbles in an electric field is more complicated. In this paper, we use the Taylor–Melcher leaky dielectric model (Melcher & Taylor 1969). This is a classical model proposed in the 1960s for studying the electrohydrodynamics of a gas bubble immersed in poorly conducting liquids where most of the charges exist only at the gas–liquid interface (Saville 1997). Accordingly, electrohydrodynamic coupling occurs only at the interface due to electric Maxwell stress. For an encapsulated bubble, the permittivities of gas and membrane are similar and much smaller than that of water. Therefore, the electric interaction of the encapsulated bubble can be well approximated by the leaky dielectric model, which was originally proposed for a gas bubble without a membrane (Lee & Kang 1999; Spelt & Matar 2006), while the mechanical properties are different for a bubble with and without a membrane. The leaky dielectric model has been validated by several experimental studies (Vizika & Saville 1992; Tsukada *et al.* 1993) and recently derived from the coupled Navier–Stokes–Poisson–Nernst–Planck (NS-PNP) framework (Schnitzer & Yariv 2015).

The encapsulating membranes for medical application are composed of polymer, albumin, galactose and lipid (Lindner 2004), with varying mechanical properties. Early studies incorporated linear elasticity (Church 1995), effective surface tension (Marmottant *et al.* 2005) and hyperelasticity (Tsiglifis & Pelekasis 2008) to investigate the dynamical behaviour of a coated bubble. Following Liu *et al.* (2011, 2012), we use a general membrane model consistent with the continuum mechanics framework, including the in-plane stress, transverse shear tension and bending moment, proposed by Barthès-Biesel & Rallison (1981) and Pozrikidis (2001), in the current study.

Using Legendre polynomials, we are able to derive a set of differential equations for the radial and shape oscillations under steady and unsteady applied electric fields, which can be solved using a numerical method. The deformed shape agrees well with experimental observations reported in the literature, under a steady electric field. Our results for an incompressible membrane with bending rigidity show that the interfacial charge distribution is determined by the magnitude of the shape modes, as well as the permittivity and conductivity of the external and internal fluids. For a hyperelastic membrane with bending rigidity, our results show that the encapsulated bubble can modulate its oscillating frequency and reach a stable shape oscillation at an appreciable amplitude.

The rest of the paper is organized as follows. In § 2, we derive the mathematical model for the electric field and flow field. These two fields are combined in stress balance at an interface (§ 2.3) and charge transport equation (§ 2.4). In § 3.1, a simplified case for a membrane with bending rigidity only is investigated and the results are compared with the experimental results by Kummrow & Helfrich (1991). In § 3.2, the dynamics of a bubble coated by a hyperelastic membrane with bending rigidity is investigated. The feasibility of applying an oscillatory electric field to find out the natural frequency of shape modes is revealed. In § 4, concluding remarks are given.

2. Problem formulation

We consider an encapsulated bubble suspended between two conducting plates parallel to each other. Applying a temporally constant or varying voltage yields a steady or oscillatory electric field. We assume the separation between the two plates is much larger than the bubble radius, so the effect of boundary confinement can

https://doi.org/10.1017/jfm.2018.170 Published online by Cambridge University Press

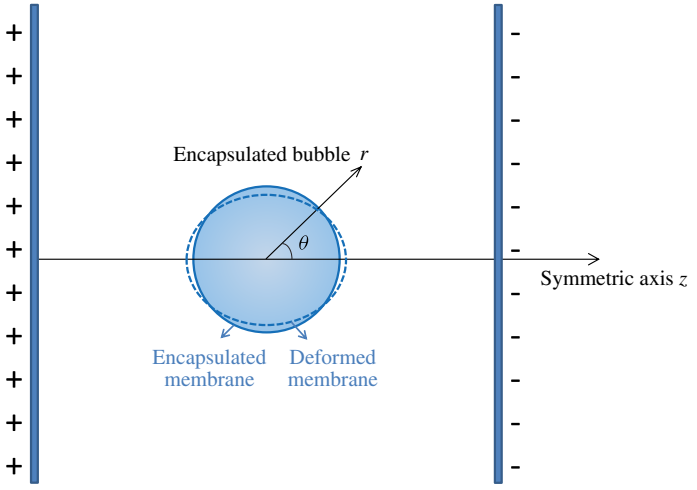


FIGURE 1. (Colour online) The coordinates of the encapsulated bubble in a spatially uniform electric field.

be neglected. The flow field and electric field are assumed to be axisymmetric with the axis of symmetry along the direction of the applied electric field z and through the centre of the bubble (figure 1). We establish a polar coordinate system with the origin at the centre of the bubble and consider a perturbation to a spherical shape. The positions of the material points at the bubble interface are thereby determined by the radial and zenith directions and expanded in terms of the (associated) Legendre polynomials as

$$r(\theta, t) = R(t) + \sum_{k=2}^{\infty} a_k(t) P_k(\cos\theta), \tag{2.1}$$

$$\Theta(\theta, t) = \theta + \frac{1}{R} \sum_{k=1}^{\infty} b_k(t) P_k^1(\cos\theta), \tag{2.2}$$

where a_k is the amplitude of the shape mode and b_k is the amplitude of the displacements of material points along the zenith direction accompanying the deformation. It is noted that the summation in (2.1) is from $k=2$ since the order of $k=1$ represents the translation of a bubble without deformation and does not account for shape modes. The summation in (2.2) is from $k=1$ in which the first-order mode b_1 denotes the extension or compression along the interface while the shape remains spherical. The surface shape function is defined as

$$S \equiv r - R(t) - \sum_{k=2}^{\infty} a_k(t) P_k(\cos\theta) = 0, \tag{2.3}$$

from which the unit normal vector $\boldsymbol{n}$ and tangential vector $\boldsymbol{t}$ are obtained:

$$\boldsymbol{n} = \frac{\nabla S}{|\nabla S|} \simeq \boldsymbol{e}_r - \boldsymbol{e}_\theta \sum_{k=2}^{\infty} \frac{a_k}{R} P_k^1(\cos\theta), \tag{2.4}$$

$$\boldsymbol{t} \simeq \boldsymbol{e}_\theta + \boldsymbol{e}_r \sum_{k=2}^{\infty} \frac{a_k}{R} P_k^1(\cos\theta). \tag{2.5}$$

https://doi.org/10.1017/jfm.2018.170 Published online by Cambridge University Press

2.1. *Electric field*

We assume that there is no free charge in the bulk, and it only exists on the bubble interface. According to Gauss's law and Faraday's law without induction, the external and internal electric fields $\boldsymbol{E}_{ex}$ and $\boldsymbol{E}_{in}$ are irrotational and solenoidal. Therefore, the electric fields can be expressed by the electric potentials as

$$\boldsymbol{E}_{ex} = -\nabla\psi_{ex}, \quad \boldsymbol{E}_{in} = -\nabla\psi_{in}, \tag{2.6a,b}$$

and the electric potentials ψ_{ex} and ψ_{in} satisfy the Laplace equations

$$\nabla^2\psi_{ex} = 0, \quad \nabla^2\psi_{in} = 0. \tag{2.7a,b}$$

The boundary conditions at the bubble interface for the electric potentials are the continuity of the tangential components of the electric fields and the jump condition for the normal components of the electric displacement vectors (Saville 1997; Lee & Kang 1999), given respectively by

$$\boldsymbol{t}\cdot\nabla\psi_{ex} = \boldsymbol{t}\cdot\nabla\psi_{in}, \tag{2.8}$$

$$-\varepsilon_{ex}\boldsymbol{n}\cdot\nabla\psi_{ex} + \varepsilon_{in}\boldsymbol{n}\cdot\nabla\psi_{in} = q/\varepsilon_0, \tag{2.9}$$

where ε_0 is the permittivity of vacuum, ε_{ex} and ε_{in} are the relative permittivities of the liquid and gas phases, respectively, and q is the interfacial charge density, which is also expanded in terms of the Legendre polynomials:

$$q = \sum_{k=0}^{\infty} q_k(t)P_k(\cos\theta). \tag{2.10}$$

Owing to the spatially uniform distribution of electric field as $r \to \infty$ and the requirement of regularity at $r = 0$, the solutions to the Laplace equations (2.7) have the forms of

$$\psi_{ex}(r,\theta,t) = -\frac{A_0}{r}P_0(\cos\theta) - \left(E_0 r + \frac{A_1(t)R(t)^3}{r^2}\right)P_1(\cos\theta) - \sum_{k=2}^{\infty}\frac{A_k(t)}{r^{k+1}}P_k(\cos\theta), \tag{2.11}$$

$$\psi_{in}(r,\theta,t) = -\sum_{k=0}^{\infty} B_k(t)r^k P_k(\cos\theta), \tag{2.12}$$

where E_0 is the magnitude of the applied electric field, which can be constant or vary with time. It is noted that A_1 is written separately from A_k ($k \geqslant 2$) in (2.11). The reason is that we want to make A_1 and E_0 the same dimension for convenience, and we will find in the following that the terms with the first-order Legendre polynomials $P_1(\cos\theta)$ are dominant in the electric field.

Substituting (2.11) and (2.12) into (2.8) and (2.9), and making use of the orthogonality of the Legendre polynomials, we obtain $A_0 = 0$. Coefficient B_0 is a constant related to the electric potential jump across the interface. We will see below that this constant does not affect the electric stress at the interface, as it depends on the electric field, which is proportional to the potential gradient. From the above boundary conditions, q_0 is obtained to be zero. The solutions to q_k ($k \geqslant 1$) will be

https://doi.org/10.1017/jfm.2018.170 Published online by Cambridge University Press

given in § 2.4. The other coefficients A_1, B_1, A_2, B_2, A_k and B_k ($k \geqslant 3$) are obtained as

$$A_1 = \frac{E_0(\varepsilon_{ex}-\varepsilon_{in})-q_1/\varepsilon_0}{2\varepsilon_{ex}+\varepsilon_{in}} - \frac{6a_2}{5R}\frac{(\varepsilon_{ex}+2\varepsilon_{in})q_1/\varepsilon_0+E_0(\varepsilon_{ex}-\varepsilon_{in})^2}{(2\varepsilon_{ex}+\varepsilon_{in})^2}, \tag{2.13}$$

$$B_1 = \frac{3\varepsilon_{ex}E_0-q_1/\varepsilon_0}{2\varepsilon_{ex}+\varepsilon_{in}} - \frac{6a_2}{5R}\frac{(-q_1/\varepsilon_0+3\varepsilon_{ex}E_0)(\varepsilon_{ex}-\varepsilon_{in})}{(2\varepsilon_{ex}+\varepsilon_{in})^2}, \tag{2.14}$$

$$A_2 = -\frac{R^4 q_2}{\varepsilon_0(3\varepsilon_{ex}+2\varepsilon_{in})} - \frac{6a_3R^3}{7}\frac{3E_0(\varepsilon_{ex}-\varepsilon_{in})^2+(\varepsilon_{ex}+5\varepsilon_{in})q_1/\varepsilon_0}{(2\varepsilon_{ex}+\varepsilon_{in})(3\varepsilon_{ex}+2\varepsilon_{in})}, \tag{2.15}$$

$$B_2 = -\frac{q_2}{R\varepsilon_0(3\varepsilon_{ex}+2\varepsilon_{in})} - \frac{3a_3}{7R^2}\frac{15E_0\varepsilon_{ex}(\varepsilon_{ex}-\varepsilon_{in})+(-7\varepsilon_{ex}+4\varepsilon_{in})q_1/\varepsilon_0}{(2\varepsilon_{ex}+\varepsilon_{in})(3\varepsilon_{ex}+2\varepsilon_{in})}, \tag{2.16}$$

$$\begin{aligned} A_k = & -\frac{R^{k+2}q_k/\varepsilon_0}{(k+1)\varepsilon_{ex}+k\varepsilon_{in}} + \frac{R^{k+1}}{2\varepsilon_{ex}+\varepsilon_{in}} \\ & \times\left\{\frac{k}{2k-1}a_{k-1}\left[3E_0(\varepsilon_{ex}-\varepsilon_{in})-\frac{q_1}{\varepsilon_0}\frac{(k+5)\varepsilon_{ex}+(2k+1)\varepsilon_{in}}{(k+1)\varepsilon_{ex}+k\varepsilon_{in}}\right]\right. \\ & \left.-\frac{k+1}{2k+3}a_{k+1}\left[\frac{3kE_0(\varepsilon_{ex}-\varepsilon_{in})^2}{(k+1)\varepsilon_{ex}+k\varepsilon_{in}}+\frac{q_1}{\varepsilon_0}\frac{(4-k)\varepsilon_{ex}+(4k+2)\varepsilon_{in}}{(k+1)\varepsilon_{ex}+k\varepsilon_{in}}\right]\right\}, \end{aligned} \tag{2.17}$$

$$\begin{aligned} B_k = & -\frac{R^{-k+1}q_k/\varepsilon_0}{(k+1)\varepsilon_{ex}+k\varepsilon_{in}} + \frac{R^{-k}}{(k+1)\varepsilon_{ex}+k\varepsilon_{in}}\left\{\frac{k(k-1)}{2k-1}a_{k-1}\frac{q_1}{\varepsilon_0}\right. \\ & \left.-\frac{k+1}{2k+3}a_{k+1}\left[\frac{3(2k+1)E_0\varepsilon_{ex}(\varepsilon_{ex}-\varepsilon_{in})}{2\varepsilon_{ex}+\varepsilon_{in}}+\frac{q_1}{\varepsilon_0}\frac{(1-4k)\varepsilon_{ex}+(k+2)\varepsilon_{in}}{2\varepsilon_{ex}+\varepsilon_{in}}\right]\right\}. \end{aligned} \tag{2.18}$$

The details of applying Legendre polynomials to the boundary conditions (2.8) and (2.9) are given in appendices A and B.

2.2. *Flow field*

We assume that the flow field inside the bubble is negligible and consider only the flow field outside the bubble by the incompressible Navier–Stokes equations:

$$\nabla\cdot\boldsymbol{u}=0, \tag{2.19}$$

$$\rho\frac{\partial\boldsymbol{u}}{\partial t}+\rho[(\boldsymbol{u}-w\boldsymbol{e}_z)\cdot\nabla]\boldsymbol{u}=-\nabla p+\mu\nabla\cdot(\nabla\boldsymbol{u}+\nabla\boldsymbol{u}^{\mathrm{T}}), \tag{2.20}$$

where $\boldsymbol{u}$ and p are the velocity and pressure, respectively, w is the translational velocity of the bubble along the z axis, and ρ and μ are the liquid density and viscosity, respectively. The velocity and pressure are decomposed into a potential part (with subscript p) and viscous pressure correction (with subscript v) as (Prosperetti 1977)

$$\boldsymbol{u}=\boldsymbol{u}_p+\boldsymbol{u}_v,\quad p=p_p+p_v. \tag{2.21a,b}$$

The potential part is obtained by the velocity potential φ, which satisfies the Laplace equation and the boundary condition:

$$\frac{\partial S}{\partial t}+(\nabla\varphi-w\boldsymbol{e}_z)\cdot\nabla S=0, \tag{2.22}$$

https://doi.org/10.1017/jfm.2018.170 Published online by Cambridge University Press

where S is the surface function defined in (2.3). The velocity potential is obtained therefrom as

$$\varphi = \sum_{k=0}^{\infty} \frac{C_k(t)}{r^{k+1}} P_k(\cos\theta), \tag{2.23}$$

where

$$C_0 = -\dot{R}R^2, \tag{2.24}$$

$$C_1 = -\frac{R^3}{2}w + \frac{3}{10}R^2 w a_2, \tag{2.25}$$

$$C_k = -\frac{R^{k+2}}{k+1}\left(\dot{a}_k + \frac{2\dot{R}a_k}{R}\right) + \frac{3k}{2}R^{k+1}w\left(\frac{a_{k+1}}{2k+3} - \frac{a_{k-1}}{2k-1}\right). \tag{2.26}$$

The velocity of the potential part is obtained consequently as

$$\boldsymbol{u}_p = \frac{\partial\varphi}{\partial r}\boldsymbol{e}_r + \frac{1}{r}\frac{\partial\varphi}{\partial\theta}\boldsymbol{e}_\theta, \tag{2.27}$$

and the pressure of the potential part is obtained by the Bernoulli equation as

$$p_p = p_\infty - \rho\left[\frac{\partial\varphi}{\partial t} + \frac{1}{2}|\nabla\varphi|^2 - w\boldsymbol{e}_z\cdot\nabla\varphi\right]. \tag{2.28}$$

The viscous correction part is solved by the toroidal component of the vorticity $T_k(r,t)$, which satisfies the linearized Navier–Stokes equation (Prosperetti 1977)

$$\rho\frac{\partial T_k}{\partial t} + \rho\frac{\partial}{\partial r}[\dot{R}(R/r)^2 T_k] - \mu\frac{\partial^2 T_k}{\partial r^2} + \mu k(k+1)r^{-2}T_k = 0. \tag{2.29}$$

The velocity and pressure are written in terms of the toroidal field as

$$\boldsymbol{u}_v = \left(\sum_{k=1}^{\infty} T_k(r,t)P_k(\cos\theta) - \frac{\partial\Phi}{\partial r}\right)\boldsymbol{e}_r - \frac{1}{r}\frac{\partial\Phi}{\partial\theta}\boldsymbol{e}_\theta, \tag{2.30}$$

$$p_v = \sum_{k=1}^{\infty} k\left\{\mu_l T_k(R,t)/R + \rho(\dot{R}/R_i)\int_R^{\infty}[(R/s)^3 - 1](R/s)^k T_k(s,t)\,\mathrm{d}s\right\}P_k(\cos\theta), \tag{2.31}$$

where

$$\begin{aligned}\Phi = \sum_{k=1}^{\infty} P_k(\cos\theta)\Bigg[&\left(-\frac{k+1}{2k+1}\int_R^{\infty} s^{-k}T_k(s,t)\,\mathrm{d}s + \frac{k+1}{2k+1}\int_R^{r} s^{-k}T_k(s,t)\,\mathrm{d}s\right)r^k \\ &+ \left(-\frac{k}{2k+1}R^{2k+1}\int_R^{\infty} s^{-k}T_k(s,t)\,\mathrm{d}s + \frac{k}{2k+1}\int_R^{r} s^{k+1}T_k(s,t)\,\mathrm{d}s\right)r^{-(k+1)}\Bigg].\end{aligned} \tag{2.32}$$

The partial differential equation (2.29) will be solved numerically subject to the boundary conditions to be discussed. The velocity $\boldsymbol{u}_v$ and pressure p_v are subsequently obtained. The detailed derivation for the flow field can be found in Liu *et al.* (2012) and Liu, Sugiyama & Takagi (2016).

https://doi.org/10.1017/jfm.2018.170 Published online by Cambridge University Press

2.3. *Stress balance at the interface*

The stress balance at the interface includes the pressure difference, the jump of the viscous and Maxwell stresses, and the membrane stress (for encapsulated bubbles only) or surface tension (for gas bubbles only), in the normal and tangential directions, respectively:

$$-p_{ex} + \boldsymbol{n}\cdot\boldsymbol{T}_{ex}\cdot\boldsymbol{n} + \boldsymbol{n}\cdot\boldsymbol{M}_{ex}\cdot\boldsymbol{n} = -p_{in} + \boldsymbol{n}\cdot\boldsymbol{M}_{in}\cdot\boldsymbol{n} + F_n, \tag{2.33}$$

$$\boldsymbol{n}\cdot\boldsymbol{T}_{ex}\cdot\boldsymbol{t} + \boldsymbol{n}\cdot\boldsymbol{M}_{ex}\cdot\boldsymbol{t} = \boldsymbol{n}\cdot\boldsymbol{M}_{in}\cdot\boldsymbol{t} + F_t, \tag{2.34}$$

where p_{ex} and p_{in} are the pressure outside and inside the bubble, respectively; $\boldsymbol{T}_{ex}$ is the viscous stress tensor at the liquid side, while the viscous stress in the bubble is neglected due to the small viscosity of gas; $\boldsymbol{M}_{ex}$ and $\boldsymbol{M}_{in}$ are the Maxwell stress tensors outside and inside the bubble, respectively; and F_n and F_t are the normal and tangential interfacial stresses, respectively. The derivations of these terms are given in detail as follows.

The external pressure p_{ex} is calculated by (2.21*b*), (2.28) and (2.31), and evaluated at the bubble interface. The interior of the bubble is gas, which is compressible. The internal pressure p_{in} is considered to be uniformly distributed, calculated by

$$p_{in} = p_{in0}\left(\frac{V_0}{V}\right)^{\Gamma}, \tag{2.35}$$

where V is the volume of the bubble, and the subscript 0 indicates the initial value; Γ is the polytropic index.

The viscous stress tensor at the liquid side $\boldsymbol{T}_{ex}$ is expressed as

$$\boldsymbol{T}_{ex} = \mu(\nabla\boldsymbol{u} + \nabla\boldsymbol{u}^{\mathrm{T}}), \tag{2.36}$$

where the velocity includes the potential part and viscous correction, given by (2.21*a*), (2.27) and (2.30). The normal and tangential components of the viscous stress are written explicitly as

$$\begin{aligned}\boldsymbol{n}\cdot\boldsymbol{T}_{ex}\cdot\boldsymbol{n} \;=\; & P_0 2\mu\left[-\frac{2\dot{R}}{R}\right] + P_1 2\mu\left[-\frac{3w}{R} + \frac{27}{5}\frac{w}{R^2}a_2 + \frac{2}{R}\int_R^\infty s^{-1}T_1(s,t)\,\mathrm{d}s\right] \\ & + \sum_{k=2}^{\infty} P_k 2\mu\left\{-(k+2)\frac{\dot{a}_k}{R} - 2(k-1)\frac{\dot{R}}{R^2}a_k \right. \\ & + \frac{w}{R^2}\left[-\frac{3k(k-1)(k+4)}{2(2k-1)}a_{k-1} + \frac{3(k+1)(k^2+2k+6)}{2(2k+3)}a_{k+1}\right] \\ & \left. + k(k+1)R^{k-2}\int_R^\infty s^{-k}T_k(s,t)\,\mathrm{d}s\right\},\end{aligned} \tag{2.37}$$

$$\begin{aligned}\boldsymbol{n}\cdot\boldsymbol{T}_{ex}\cdot\boldsymbol{t} \;=\; & P_1^1 2\mu\left[\frac{3w}{2R} - \frac{9wa_2}{10R^2} - \frac{T_1(R,t)}{2R} - \frac{1}{R}\int_R^\infty s^{-1}T_1(s,t)\,\mathrm{d}s\right] \\ & + \sum_{k=2}^{\infty} P_k^1 2\mu\left[\frac{k+2}{k+1}\frac{\dot{a}_k}{R} + \frac{1-k}{k+1}\frac{\dot{R}a_k}{R^2} + \frac{3k(k+2)}{2}\frac{w}{R^2}\left(\frac{a_{k-1}}{2k-1} - \frac{a_{k+1}}{2k+3}\right)\right. \\ & \left. - \frac{T_k(R,t)}{2R} - R^{k-2}\int_R^\infty s^{-k}T_k(s,t)\,\mathrm{d}s\right].\end{aligned} \tag{2.38}$$

https://doi.org/10.1017/jfm.2018.170 Published online by Cambridge University Press

The Maxwell stress tensor in the liquid $\boldsymbol{M}_{ex}$ is given by the electric field as (Landau, Lifshitz & Pitaevskii 1984)

$$\boldsymbol{M}_{ex} = \varepsilon_{ex}\varepsilon_0(\boldsymbol{E}_{ex}\boldsymbol{E}_{ex} - \tfrac{1}{2}|\boldsymbol{E}_{ex}|^2\boldsymbol{I}). \tag{2.39}$$

Written in terms of the electric potential by using (2.6), the normal and tangential components of the Maxwell stress (2.39) become

$$\boldsymbol{n}\cdot\boldsymbol{M}_{ex}\cdot\boldsymbol{n} = \varepsilon_{ex}\varepsilon_0\left\{\frac{1}{2}\left[\left(\frac{\partial\psi_{ex}}{\partial r}\right)^2 - \left(\frac{1}{r}\frac{\partial\psi_{ex}}{\partial\theta}\right)^2\right] - \frac{2}{r^2}\frac{\partial\psi_{ex}}{\partial r}\frac{\partial\psi_{ex}}{\partial\theta}\sum_{k=2}^{\infty}a_kP_k^1\right\}, \tag{2.40}$$

$$\boldsymbol{n}\cdot\boldsymbol{M}_{ex}\cdot\boldsymbol{t} = \varepsilon_{ex}\varepsilon_0\left\{\frac{1}{r}\frac{\partial\psi_{ex}}{\partial r}\frac{\partial\psi_{ex}}{\partial\theta} + \frac{1}{r}\left[\left(\frac{\partial\psi_{ex}}{\partial r}\right)^2 - \left(\frac{1}{r}\frac{\partial\psi_{ex}}{\partial\theta}\right)^2\right]\sum_{k=2}^{\infty}a_kP_k^1\right\}. \tag{2.41}$$

Substituting in the expressions of electric potential (2.11), and the relations of the Legendre polynomials in appendix A, the components of the Maxwell stress at the liquid side of the interface are written explicitly as

$$\begin{aligned}
\boldsymbol{n}\cdot\boldsymbol{M}_{ex}\cdot\boldsymbol{n} \;=\; & \varepsilon_{ex}\varepsilon_0\left\{\frac{1}{2}(E_0-2A_1)^2P_1^2 - \frac{1}{2}(E_0+A_1)^2\left(\frac{\mathrm{d}P_1}{\mathrm{d}\theta}\right)^2\right.\\
& + \sum_{k=2}^{\infty}\left[\frac{6A_1}{R}(E_0-2A_1)a_kP_1^2P_k - \frac{k+1}{R^{k+2}}(E_0-2A_1)A_kP_1P_k\right.\\
& + \frac{3A_1}{R}a_k(E_0+A_1)P_k\left(\frac{\mathrm{d}P_1}{\mathrm{d}\theta}\right)^2 - \frac{A_k}{R^{k+2}}(E_0+A_1)\frac{\mathrm{d}P_1}{\mathrm{d}\theta}\frac{\mathrm{d}P_k}{\mathrm{d}\theta}\\
& \left.\left. - \frac{2}{R}(E_0-2A_1)(E_0+A_1)a_kP_1\frac{\mathrm{d}P_1}{\mathrm{d}\theta}\frac{\mathrm{d}P_k}{\mathrm{d}\theta}\right]\right\}\\
= \; & P_0\varepsilon_{ex}\varepsilon_0\left\{\frac{1}{6}(2A_1^2 - 8E_0A_1 - E_0^2) - \frac{4}{5}E_0(E_0-2A_1)\frac{a_2}{R}\right\}\\
& + P_1\varepsilon_{ex}\varepsilon_0\left\{-(2E_0-A_1)\frac{6A_2}{5R^4}\right\}\\
& + P_2\varepsilon_{ex}\varepsilon_0\left\{\frac{1}{3}(5A_1^2 - 2A_1E_0 + 2E_0^2) + (A_1-2E_0)\frac{12A_3}{7R^5}\right.\\
& \left. + \frac{2a_2}{7R}(-11A_1^2 + 20A_1E_0 - 2E_0^2)\right\}\\
& + \sum_{k=3}^{\infty}P_k\varepsilon_{ex}\varepsilon_0\left\{(A_1-2E_0)\frac{(k+1)(k+2)}{(2k+3)R^{k+3}}A_{k+1} + [A_1(3k-1) - E_0]\right.\\
& \times \frac{kA_{k-1}}{(2k-1)R^{k+1}} + [A_1^2(-6k^2-6k+3) + A_1E_0(11k^2+11k-6)\\
& - E_0^2k(k+1)]\frac{2}{(2k-1)(2k+3)}\frac{a_k}{R} + (2A_1-E_0)[kA_1 + (k+3)E_0]\\
& \times \frac{2(k+1)(k+2)}{(2k+3)(2k+5)}\frac{a_{k+2}}{R} - (2A_1-E_0)[(k+1)A_1 + (k-2)E_0]\\
& \left.\times \frac{2k(k-1)}{(2k-3)(2k-1)}\frac{a_{k-2}}{R}\right\},
\end{aligned} \tag{2.42}$$

https://doi.org/10.1017/jfm.2018.170 Published online by Cambridge University Press

$$\boldsymbol{n}\cdot\boldsymbol{M}_{ex}\cdot\boldsymbol{t}=\sum_{k=2}^{\infty}\varepsilon_{ex}\varepsilon_0\left[\frac{1}{3}(2A_1^2-8A_1E_0-E_0^2)\frac{a_k}{R}\right]P_k^1(\cos\theta). \tag{2.43}$$

The Maxwell stress in the bubble is calculated in a similar way as (2.39), (2.40) and (2.41) with the subscript replaced by '*in*'. By substituting (2.6), and (2.12), the normal and tangential components of the Maxwell stress at the gas side of the interface are written as

$$\begin{aligned}\boldsymbol{n}\cdot\boldsymbol{M}_{in}\cdot\boldsymbol{n} &= \varepsilon_{in}\varepsilon_0\left\{\frac{1}{2}B_1^2P_1^2-\frac{1}{2}B_1^2\left(\frac{\mathrm{d}P_1}{\mathrm{d}\theta}\right)^2\right.\\ &\quad\left.+\sum_{k=2}^{\infty}\left[B_1B_kkR^{k-1}P_1P_k-B_1B_kR^{k-1}\frac{\mathrm{d}P_1}{\mathrm{d}\theta}\frac{\mathrm{d}P_k}{\mathrm{d}\theta}-\frac{2B_1^2}{R}a_kP_1\frac{\mathrm{d}P_1}{\mathrm{d}\theta}\frac{\mathrm{d}P_k}{\mathrm{d}\theta}\right]\right\}\\ &= P_0\varepsilon_{in}\varepsilon_0\left[-\frac{1}{6}B_1^2-\frac{4}{5}B_1^2\frac{a_2}{R}\right]+P_1\varepsilon_{in}\varepsilon_0\left[-\frac{2}{5}RB_1B_2\right]\\ &\quad+P_2\varepsilon_{in}\varepsilon_0\left[\frac{2}{3}B_1^2-\frac{3}{7}R^2B_1B_3-\frac{4}{7R}B_1^2a_2\right]\\ &\quad+\sum_{k=3}^{\infty}P_k\varepsilon_{in}\varepsilon_0\left[-\frac{k+1}{2k+3}B_1B_{k+1}R^k+\frac{2k(k-1)}{2k-1}B_1B_{k-1}R^{k-2}\right.\\ &\quad-\frac{2k(k+1)}{(2k-1)(2k+3)}B_1^2\frac{a_k}{R}-\frac{2(k+1)(k+2)(k+3)}{(2k+3)(2k+5)}B_1^2\frac{a_{k+2}}{R}\\ &\quad\left.+\frac{2k(k-1)(k-2)}{(2k-3)(2k-1)}B_1^2\frac{a_{k-2}}{R}\right],\end{aligned} \tag{2.44}$$

$$\boldsymbol{n}\cdot\boldsymbol{M}_{in}\cdot\boldsymbol{t}=\sum_{k=2}^{\infty}\varepsilon_{in}\varepsilon_0\left[-\frac{1}{3}B_1^2\frac{a_k}{R}\right]P_k^1(\cos\theta). \tag{2.45}$$

In the general case, the membrane stress $\boldsymbol{F}$ includes the in-plane stress and bending moment (Green & Adkins 1960)

$$\boldsymbol{F}=-(\boldsymbol{P}\cdot\nabla)\cdot(\boldsymbol{\tau}+\boldsymbol{Q}\boldsymbol{n}), \tag{2.46}$$

where $\boldsymbol{P}$ $(=\boldsymbol{I}-\boldsymbol{n}\boldsymbol{n})$ is the tangential projection operator, $\boldsymbol{\tau}$ $(=\tau_\theta\boldsymbol{e}_\theta\boldsymbol{e}_\theta+\tau_\phi\boldsymbol{e}_\phi\boldsymbol{e}_\phi)$ is the in-plane stress and $\boldsymbol{Q}$ is the transverse shear tension, associated with the bending moment $\boldsymbol{m}$ $(=m_\theta\boldsymbol{e}_\theta\boldsymbol{e}_\theta+m_\phi\boldsymbol{e}_\phi\boldsymbol{e}_\phi)$ as

$$\boldsymbol{Q}=[(\boldsymbol{P}\cdot\nabla)\cdot\boldsymbol{m}]\cdot\boldsymbol{P}. \tag{2.47}$$

For a hyperelastic membrane, we adopt the strain energy function W_s to connect the in-plane stress τ_i and strain λ_i, and the bending energy function W_b to connect the bending moment m_i and the bending strain K_i:

$$\tau_i=\frac{\lambda_i}{\lambda_\theta\lambda_\phi}\frac{\partial W_s(\lambda_\theta,\lambda_\phi)}{\partial\lambda_i}, \tag{2.48}$$

$$m_i=\frac{\lambda_i}{\lambda_\theta\lambda_\phi}\frac{\partial W_b(K_\theta,K_\phi)}{\partial K_i}, \tag{2.49}$$

https://doi.org/10.1017/jfm.2018.170 Published online by Cambridge University Press

where i is chosen as θ and ϕ alternatively to represent the two principal directions. Bending strain K_i is defined as

$$K_i = \lambda_i \kappa_i - \kappa_i^R \tag{2.50}$$

to consider the effect of in-plane strain on the bending moment, where κ_i is the principal curvature, calculated by the curvature tensor $\boldsymbol{B} = \boldsymbol{P} \cdot \nabla \boldsymbol{n}$ to be

$$\kappa_\theta = \frac{1}{R} - \sum_{k=2}^{\infty} \frac{a_k}{R^2} \left(P_k + \frac{\mathrm{d}^2 P_k}{\mathrm{d}\theta^2} \right), \tag{2.51}$$

$$\kappa_\phi = \frac{1}{R} - \sum_{k=2}^{\infty} \frac{a_k}{R^2} \left(P_k + \frac{\cos\theta}{\sin\theta} P_k^1 \right). \tag{2.52}$$

As an example, we adopt the neo-Hookean law, a simple form of the strain-softening Mooney–Rivlin law (Mooney 1940), of which the strain energy function is given by

$$W_s = \frac{G_s}{2} \left(\lambda_\theta^2 + \lambda_\phi^2 + \frac{1}{\lambda_\theta^2 \lambda_\phi^2} - 3 \right), \tag{2.53}$$

where G_s is the surface modulus of elasticity. The bending strain energy function is given by the Love law (Love 1888)

$$W_b = \frac{G_b}{2} (K_\theta^2 + 2\upsilon K_\theta K_\phi + K_\phi^2), \tag{2.54}$$

where G_b is the bending modulus and υ the Poisson ratio.

Accordingly, the normal and tangential components of the membrane stress are (Liu *et al.* 2016)

$$\begin{aligned} F_n = {} & \frac{2G_s(R^6 - R_0^6)}{R^7} + \left[-12G_s \frac{R_0^6}{R^8} b_1 - 2(1+\upsilon) G_b \frac{b_1}{R^4} \right] P_1(\cos\theta) \\ & + \sum_{k=2}^{\infty} \left\{ -\frac{G_s}{R^8} [2(R^6 - 7R_0^6) a_k + 6k(k+1) R_0^6 b_k] \right. \\ & \left. + \frac{G_b}{R^4} [k(k+1)(k^2 + k - 1 + \upsilon)(a_k - b_k)] \right\} P_k(\cos\theta), \end{aligned} \tag{2.55}$$

$$\begin{aligned} F_t = {} & \left[6G_s \frac{R_0^6}{R^8} b_1 + (1+\upsilon) \frac{G_b}{R^4} b_1 \right] P_1^1(\cos\theta) \\ & + \sum_{k=2}^{\infty} \left\{ \frac{G_s}{R^8} [(R^6 - 7R_0^6) a_k + (3k(k+1) R_0^6 + (k-1)(k+2) R^6) b_k] \right. \\ & \left. - \frac{G_b}{R^4} (k^2 + k - 1 + \upsilon)(a_k - b_k) \right\} P_k^1(\cos\theta). \end{aligned} \tag{2.56}$$

The expressions for the interfacial stresses F_n and F_t can be specified depending on constitutive laws for different types of interface. In the following part of this section we keep this notation in the equations and only add superscripts to denote the expansion at specific order of the Legendre polynomials.

https://doi.org/10.1017/jfm.2018.170 Published online by Cambridge University Press

We substitute (2.35)–(2.38) and (2.42)–(2.45) into (2.33) and (2.34) and expand them with respect to the Legendre polynomials. Utilizing the orthogonality of the polynomials, we obtain dynamic equations at different orders. The zeroth order of (2.33) provides the dynamics of radial oscillation:

$$R\ddot{R}+\frac{3}{2}\dot{R}^2+\frac{1}{\rho}\left(p_\infty-p_{in}+4\mu_l\frac{\dot{R}}{R}\right)-\frac{1}{4}w^2-\frac{1}{\rho}\varepsilon_{in}\varepsilon_0B_1^2\left(\frac{1}{6}+\frac{4a_2}{5R}\right)$$
$$-\frac{1}{\rho}\varepsilon_{ex}\varepsilon_0\left[\frac{1}{6}(2A_1^2-8E_0A_1-E_0^2)-\frac{4}{5}E_0(E_0-2A_1)\frac{a_2}{R}\right]+\frac{F_n^0}{\rho}=0, \tag{2.57}$$

which is a Rayleigh–Plesset type equation with translational motion and interfacial stresses. We note that the Maxwell stress, as a driving force, is quadratic in electric field strength E_0, shown by substituting the expressions of A_1 (2.13) and B_1 (2.14) into (2.57). This implies that the oscillatory frequency of the radial mode is twice the frequency of the oscillatory electric field.

The coefficients before the first-order Legendre polynomials $P_1(\cos\theta)$ in (2.33) provide the translational equation:

$$\frac{1}{2}R\dot{w}+\frac{3}{2}\dot{R}w-\frac{7}{10}\dot{w}a_2-\frac{9}{10}w\dot{a}_2-\frac{6}{5}\frac{\dot{R}}{R}wa_2$$
$$+\frac{\mu_lT_1(R,t)}{\rho R}+\frac{\dot{R}}{R}\int_R^\infty\left[\left(\frac{R}{s}\right)^3-1\right]\left(\frac{R}{s}\right)T_1(s,t)\,\mathrm{d}s$$
$$+\frac{2\mu_l}{\rho}\left(\frac{3w}{R}-\frac{27}{5}\frac{a_2}{R^2}w-\frac{2}{R}\int_R^\infty s^{-1}T_1(s,t)\,\mathrm{d}s\right)$$
$$-\frac{2}{5\rho}\varepsilon_{in}\varepsilon_0RB_1B_2+\frac{1}{\rho}\varepsilon_{ex}\varepsilon_0(2E_0-A_1)\frac{6A_2}{5R^4}+\frac{F_n^1}{\rho}=0, \tag{2.58}$$

where the first two terms are associated with the inertia of added mass, and the terms of the second and third lines are the drag due to viscosity. The translational motion is induced by the applied electric field. From the first two terms in the last line, we know that the Maxwell stress at this order is proportional to the coefficients A_2 and B_2. By investigating the expressions (2.15) and (2.16), if the even-order charge distribution and odd-order shape mode are not triggered, which will be demonstrated below, the driving force of the electric field on the translational motion is zero, i.e. the bubble does not translate under a spatially uniform electric field.

The equations of the second-order shape oscillation and the kth-order shape oscillation ($k\geqslant 3$) are

$$\frac{1}{3}R\ddot{a}_2+\dot{R}\dot{a}_2+\left(-\frac{1}{3}\ddot{R}-\frac{183}{70}\frac{w^2}{R}\right)a_2+\frac{3}{4}w^2-\frac{15}{14}w\dot{a}_3-a_3\left(\frac{9}{7}\frac{\dot{R}}{R}w+\frac{6}{7}\dot{w}\right)$$
$$+\frac{2\mu_lT_2(R,t)}{\rho R}+\frac{2\dot{R}}{R}\int_R^\infty\left[\left(\frac{R}{s}\right)^3-1\right]\left(\frac{R}{s}\right)^2T_2(s,t)\,\mathrm{d}s$$
$$+\frac{2\mu_l}{\rho}\left[4\frac{\dot{a}_2}{R}+\frac{2\dot{R}}{R^2}a_2-\frac{9a_3}{R^2}w-6\int_R^\infty s^{-2}T_2(s,t)\,\mathrm{d}s\right]$$
$$+\frac{1}{\rho}\varepsilon_{in}\varepsilon_0\left(\frac{2}{3}B_1^2-\frac{3}{7}R^2B_1B_3-\frac{4}{7R}B_1^2a_2\right)$$

https://doi.org/10.1017/jfm.2018.170 Published online by Cambridge University Press

$$-\frac{1}{\rho}\varepsilon_{ex}\varepsilon_0\left[\frac{1}{3}(5A_1^2-2A_1E_0+2E_0^2)+(A_1-2E_0)\frac{12A_3}{7R^5}\right.$$
$$\left.+\frac{2a_2}{7R}(-11A_1^2+20A_1E_0-2E_0^2)\right]+\frac{F_n^2}{\rho}=0, \tag{2.59}$$

$$\frac{1}{k+1}R\ddot{a}_k+\left[\frac{3\dot{R}}{k+1}+\frac{2(k+2)\mu_l}{\rho R}\right]\dot{a}_k$$
$$+\left[-\frac{k-1}{k+1}\ddot{R}+\frac{4(k-1)\mu_l}{\rho}\frac{\dot{R}}{R^2}-\frac{9(2k^4+3k^3+k^2+k-1)}{2(2k-1)(2k+1)(2k+3)}\frac{w^2}{R}\right]a_k$$
$$+\dot{a}_{k-1}\frac{3}{2}w+a_{k-1}\left[\frac{3(k-1)\dot{R}w}{(2k-1)R}+\frac{k}{2(2k-1)}\dot{w}\right]-\dot{a}_{k+1}\frac{3(2k+1)}{2(2k+3)}w$$
$$-a_{k+1}\left[\frac{3(k+1)w\dot{R}}{(2k+3)R}+\frac{5k+2}{2(2k+3)}\dot{w}\right]$$
$$+\frac{k\mu_l T_k(R,t)}{\rho R}+k\frac{\dot{R}}{R}\int_R^\infty\left[\left(\frac{R}{s}\right)^3-1\right]\left(\frac{R}{s}\right)^k T_k(s,t)\,\mathrm{d}s$$
$$+\frac{2\mu_l}{\rho}\left\{\frac{w}{R^2}\left[\frac{3k(k-1)(k+4)}{2(2k-1)}a_{k-1}-\frac{3(k+1)(k^2+2k+6)}{2(2k+3)}a_{k+1}\right]\right.$$
$$\left.-k(k+1)R^{k-2}\int_R^\infty s^{-k}T_k(s,t)\,\mathrm{d}s\right\}$$
$$+\frac{1}{\rho}\varepsilon_{in}\varepsilon_0\left[-\frac{k+1}{2k+3}B_1B_{k+1}R^k+\frac{2k(k-1)}{2k-1}B_1B_{k-1}R^{k-2}-\frac{2k(k+1)}{(2k-1)(2k+3)}\frac{B_1^2}{R}a_k\right.$$
$$\left.-\frac{2(k+1)(k+2)(k+3)}{(2k+3)(2k+5)}B_1^2\frac{a_{k+2}}{R}+\frac{2k(k-1)(k-2)}{(2k-3)(2k-1)}B_1^2\frac{a_{k-2}}{R}\right]$$
$$-\frac{1}{\rho}\varepsilon_{ex}\varepsilon_0\left\{(A_1-2E_0)\frac{(k+1)(k+2)}{(2k+3)R^{k+3}}A_{k+1}+[A_1(3k-1)-E_0]\frac{kA_{k-1}}{(2k-1)R^{k+1}}\right.$$
$$+[A_1^2(-6k^2-6k+3)+A_1E_0(11k^2+11k-6)-E_0^2k(k+1)]\frac{2}{(2k-1)(2k+3)}\frac{a_k}{R}$$
$$+(2A_1-E_0)[kA_1+(k+3)E_0]\frac{2(k+2)(k+2)}{(2k+3)(2k+5)}\frac{a_{k+2}}{R}$$
$$\left.+(2A_1-E_0)[(k+1)A_1+(k-2)E_0]\frac{2k(k-1)}{(2k-3)(2k-1)}\frac{a_{k-2}}{R}\right\}+\frac{F_n^k}{\rho}=0. \tag{2.60}$$

The equation for the second-order shape mode is written separately since the shape oscillation equation is related to the adjacent shape modes, and the lower-order shape mode to the $k=2$ mode is the translational motion, denoted by its velocity. In addition, the following results will show that the second-order shape mode is dominant under an electric field.

To solve the toroidal field (2.29) numerically, a boundary condition at the bubble interface is needed. Here we use the tangential stress balance (2.34) and write it in terms of different modes as

$$2\mu\left[\frac{3w}{2R}-\frac{9wa_2}{10R^2}-\frac{T_1(R,t)}{2R}-\frac{1}{R}\int_R^\infty s^{-1}T_1(s,t)\,\mathrm{d}s\right]=F_t^1 \tag{2.61}$$

https://doi.org/10.1017/jfm.2018.170 Published online by Cambridge University Press

for $k=1$, and as

$$2\mu\left[\frac{k+2}{k+1}\frac{\dot{a}_k}{R}+\frac{1-k}{k+1}\frac{\dot{R}a_k}{R^2}+\frac{3k(k+2)}{2}\frac{w}{R^2}\left(\frac{a_{k-1}}{2k-1}-\frac{a_{k+1}}{2k+3}\right)\right.$$
$$\left.-\frac{T_k(R,t)}{2R}-R^{k-2}\int_R^\infty s^{-k}T_k(s,t)\,\mathrm{d}s\right]+\varepsilon_{ex}\varepsilon_0\left[\frac{1}{3}(2A_1^2-8A_1E_0-E_0^2)\frac{a_k}{R}\right]$$
$$+\varepsilon_{in}\varepsilon_0\left[\frac{1}{3}B_1^2\frac{a_k}{R}\right]=F_t^k \tag{2.62}$$

for $k\geqslant 2$.

For a bubble encapsulated with a hyperelastic membrane, the material points at the surface move along the tangential direction as well as the normal direction during deformation. Therefore, the tangential displacement (2.2) should be solved. To completely determine the system of equations, a no-slip condition at the interface, i.e. the continuity of the tangential velocity, is applied (Liu *et al.* 2016)

$$-\frac{1}{k+1}\dot{a}_k-\frac{2\dot{R}a_k}{(k+1)R}-\frac{3k}{2R}w\left(\frac{a_{k-1}}{2k-1}-\frac{a_{k+1}}{2k+3}\right)+R_i^{k-1}\int_R^\infty s^{-k}T_k(s,t)\,\mathrm{d}s=\dot{b}_k-\frac{\dot{R}b_k}{R}. \tag{2.63}$$

So far, the dynamic equations for the radial oscillation, translation and shape oscillation have been derived and will be solved by using the fourth-order Runge–Kutta method with the static initial condition. The distribution of free charge q_k at the interface, which is embedded in A_k and B_k (2.13)–(2.18), will be solved in the next section.

2.4. *Free charge on the interface*

In this section, we consider the transport of free charge on the interface caused by the jump of current across the interface and the stretching of the interface. The conservation of charge, written in the integral form, is

$$\int_{S(t)}(\kappa_{ex}\boldsymbol{n}\cdot\nabla\psi_{ex}-\kappa_{in}\boldsymbol{n}\cdot\nabla\psi_{in})\,\mathrm{d}S=\frac{\mathrm{d}}{\mathrm{d}t}\int_{S(t)}q\,\mathrm{d}S, \tag{2.64}$$

where κ_{ex} and κ_{in} are the conductivity of the liquid and gas phase. It is noted that (2.64) is established based on the local coordinate with origin at the centre of the bubble. Therefore we use the relative velocity

$$\bar{\boldsymbol{u}}=\boldsymbol{u}-w\boldsymbol{e}_z \tag{2.65}$$

in the following to establish the dynamic equation for the charge distribution based on a frame of reference moving with the bubble centre.

The area of the interface may be changed under an electric field. Therefore, the time derivative of the area should be considered as shown on the right-hand side of (2.64) or written explicitly as

$$\frac{\mathrm{d}}{\mathrm{d}t}\int_{S(t)}q\,\mathrm{d}S=\int_{S(t)}\left(\frac{\mathrm{d}q}{\mathrm{d}t}\,\mathrm{d}S+q\frac{\mathrm{d}}{\mathrm{d}t}\,\mathrm{d}S\right), \tag{2.66}$$

https://doi.org/10.1017/jfm.2018.170 Published online by Cambridge University Press

where the second term on the right-hand side is treated using Batchelor's method (Batchelor 2000) to calculate the time derivative of a material surface element with vector area d$\boldsymbol{S}$:

$$\frac{\mathrm{d}}{\mathrm{d}t}\,\mathrm{d}\boldsymbol{S} = \mathrm{d}S\,\nabla\cdot\bar{\boldsymbol{u}} - (\nabla\bar{\boldsymbol{u}})\cdot\mathrm{d}\boldsymbol{S}. \tag{2.67}$$

Writing $\mathrm{d}\boldsymbol{S} = \boldsymbol{n}\,\mathrm{d}S$ and taking the inner product of $\boldsymbol{n}$ to the above equation yields (Stone 1990)

$$\frac{\mathrm{d}}{\mathrm{d}t}\,\mathrm{d}S = \mathrm{d}S\,\nabla_s\cdot\bar{\boldsymbol{u}}. \tag{2.68}$$

Since the material surface element $S(t)$ is arbitrary, the integrals of (2.64) can be eliminated,

$$\kappa_{ex}\boldsymbol{n}\cdot\nabla\psi_{ex} - \kappa_{in}\boldsymbol{n}\cdot\nabla\psi_{in} = \frac{\mathrm{d}q}{\mathrm{d}t} + q\nabla_s\cdot\bar{\boldsymbol{u}}. \tag{2.69}$$

The Lagrangian derivative to the charge density is written as

$$\frac{\mathrm{d}q}{\mathrm{d}t} = \frac{\partial\widetilde{q}}{\partial t} + (\bar{\boldsymbol{u}}\cdot\nabla)\widetilde{q}, \tag{2.70}$$

where q should be extended to the neighbourhood of the interface, denoted by $\widetilde{q}$, in order to calculate the derivative (Pereira *et al.* 2007), as the charge only exists on the interface.

Decomposing $\bar{\boldsymbol{u}}$ into the tangential and normal components,

$$\bar{\boldsymbol{u}} = \bar{\boldsymbol{u}}_s + \bar{\boldsymbol{u}}_n = \bar{\boldsymbol{u}}_s + (\bar{\boldsymbol{u}}\cdot\boldsymbol{n})\boldsymbol{n}, \tag{2.71}$$

the right-hand side of (2.69) can be written as

$$\frac{\mathrm{d}q}{\mathrm{d}t} + q\nabla_s\cdot\bar{\boldsymbol{u}} = \frac{\partial q}{\partial t} + \bar{\boldsymbol{u}}_n\cdot\boldsymbol{e}_\theta\frac{1}{r}\frac{\partial q}{\partial\theta} + \nabla_s\cdot(q\bar{\boldsymbol{u}}_s) + q(\nabla_s\cdot\boldsymbol{n})(\bar{\boldsymbol{u}}\cdot\boldsymbol{n}). \tag{2.72}$$

The detailed derivation of (2.72) is deferred to appendix C. Thus the charge transport equation (2.69) can be written explicitly for different modes as

$$\begin{aligned}&\dot{q}_1 + q_1\left(\frac{2\dot{R}}{R} + \frac{6\dot{a}_2}{5R}\right) - q_2\left(\frac{3w}{5R} - \frac{2}{5R}\int_R^\infty s^{-1}T_1(s,t)\,\mathrm{d}s\right)\\ &\quad= \kappa_{in}\left(B_1 - \frac{6}{5}\frac{B_1}{R}a_2\right) - \kappa_{ex}\left[(E_0 - 2A_1) + \frac{6}{5}\frac{a_2}{R}(A_1 - E_0)\right],\end{aligned} \tag{2.73}$$

$$\begin{aligned}&\dot{q}_2 + q_2\frac{2\dot{R}}{R} + q_1\left[\frac{3w}{R} - \left(\frac{2}{R} + \frac{4a_2}{7R^2}\right)\int_R^\infty s^{-1}T_1(s,t)\,\mathrm{d}s + \frac{6\dot{R}a_3}{7R^2} + \frac{12\dot{a}_3}{7R}\right]\\ &\quad - q_3\left(\frac{9w}{7R} - \frac{6}{7R}\int_R^\infty s^{-1}T_1(s,t)\,\mathrm{d}s\right)\\ &\quad= \kappa_{in}\left(2B_2R - \frac{12}{7}\frac{B_1}{R}a_3\right) - \kappa_{ex}\left[-\frac{3A_2}{R^4} + \frac{6}{7}\frac{a_3}{R}(A_1 - 2E_0)\right],\end{aligned} \tag{2.74}$$

$$\dot{q}_k + q_k\frac{2\dot{R}}{R} + q_1\left[-\frac{2k(k+1)}{(2k-1)(2k+3)}\frac{a_k}{R^2}\int_R^\infty s^{-1}T_1(s,t)\,\mathrm{d}s + \frac{(k+2)(k+1)}{(2k+3)}\frac{\dot{a}_{k+1}}{R}\right.$$

https://doi.org/10.1017/jfm.2018.170 Published online by Cambridge University Press

$$+\frac{k^2+2k-1}{2k-1}\frac{\dot{a}_{k-1}}{R}+\frac{2(k^2-1)}{2k+3}\frac{\dot{R}}{R^2}a_{k+1}+\frac{2(k^2-k-1)}{2k-1}\frac{\dot{R}}{R^2}a_{k-1}\Bigg]$$
$$+\left(q_{k-1}\frac{k(k+1)}{2k-1}-q_{k+1}\frac{k(k+1)}{2k+3}\right)\left(\frac{3w}{2R}-\frac{1}{R}\int_R^\infty s^{-1}T_1(s,t)\,\mathrm{d}s\right)$$
$$=\kappa_{in}\left[kB_kR^{k-1}-\frac{B_1}{R}\left(\frac{(k+1)(k+2)}{2k+3}a_{k+1}-\frac{k(k-1)}{2k-1}a_{k-1}\right)\right]$$
$$-\kappa_{ex}\left[-(k+1)\frac{A_k}{R^{k+2}}+\frac{a_{k-1}}{R}\frac{k}{2k-1}\left((k+5)A_1+(k-1)E_0\right)\right.$$
$$\left.-\frac{a_{k+1}}{R}\frac{k+1}{2k+3}\left((k-4)A_1+(k+2)E_0\right)\right]. \tag{2.75}$$

These equations will be solved together with the dynamic equations derived in § 2.3 by using the fourth-order Runge–Kutta method assuming no free charge in the initial state.

3. Results

In this section, we first present our results for a bubble coated with a bending-resistant membrane and compare them with experimental observations in Kummrow & Helfrich (1991). Afterwards, we show our results for a bubble coated with a hyperelastic and bending-resistant membrane. The external fluid is assumed to be water, with density $\rho = 1000$ kg m^{-3}, viscosity $\mu = 0.001$ kg m^{-1} s^{-1}, relative permittivity $\varepsilon_{ex} = 81$ and conductivity $\kappa_{ex} = 5 \times 10^{-4}$ S m^{-1}. The internal fluid is considered as gas, with relative permittivity $\varepsilon_{in} = 1$ and conductivity $\kappa_{in} = 3 \times 10^{-15}$ S m^{-1}. The ambient pressure is set as $p_\infty = 10^5$ Pa. The polytropic index Γ is calculated to be 1.2 using (3.24)–(3.28) in Prosperetti (1991).

3.1. *A bubble coated with a bending-resistant membrane*

To validate our model, we first investigate the effects of electric stress and membrane stress on the bubble shape. Owing to the lack of experimental results for encapsulated bubbles, we compare with the results by Kummrow & Helfrich (1991), which are for a vesicle coated with a lipid bilayer and which only bears bending rigidity. Accordingly, we modify our membrane model to exclude hyperelastic stress and only consider the bending moments. The in-plane strain λ_i is prescribed to be 1, implying the membrane is tensionless. For this case, the effect of gas compressibility on the bubble dynamics is small. Therefore, the results of a vesicle and an encapsulated bubble can be compared, although the inside of a vesicle is not gas and the compositions of encapsulating membranes are different. If we set the Poisson ratio υ to be zero, which is the case for a material with small lateral expansion when compressed, the bending strain energy function (2.54) is equivalent to Helfrich's energy function (Helfrich 1973), and applicable to the vesicle used in Kummrow & Helfrich (1991). The membrane stress (2.46) is reduced to

$$\boldsymbol{F} = -(\boldsymbol{P}\cdot\nabla)\cdot\boldsymbol{Q}\boldsymbol{n}, \tag{3.1}$$

and the bending moments become

$$m_\theta = G_b(\kappa_\theta - \kappa_\theta^R), \quad m_\phi = G_b(\kappa_\phi - \kappa_\phi^R). \tag{3.2a,b}$$

https://doi.org/10.1017/jfm.2018.170 Published online by Cambridge University Press

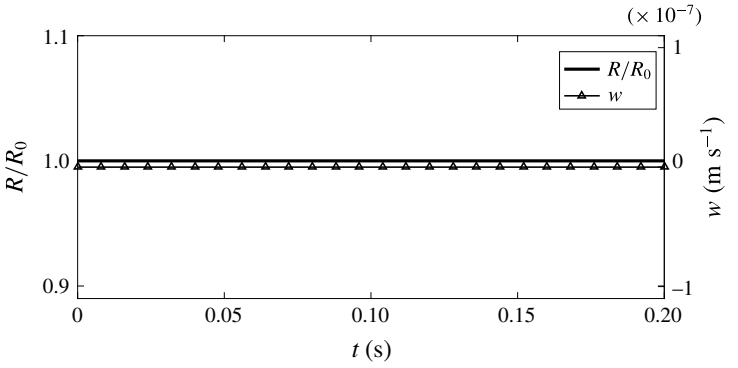


FIGURE 2. Time evolutions of radius (left y-axis) and velocity (right y-axis) of an encapsulated bubble with initial radius $R_0 = 23$ μm and bending modulus $G_b = 2.47 \times 10^{-20}$ N m under a steady electric field with $E_0 = 10^4$ V m^{-1}.

The normal and tangential components of the membrane stress are obtained as

$$F_n = \sum_{k=2}^{\infty} G_b \frac{a_k}{R^4} k(k-1)(k+1)(k+2)P_k, \tag{3.3}$$

$$F_t = -\sum_{k=2}^{\infty} G_b \frac{a_k}{R^4} (k-1)(k+2)P_k^1. \tag{3.4}$$

According to Kummrow & Helfrich (1991), we choose a bubble with initial radius $R_0 = 23$ μm and bending modulus $G_b = 2.47 \times 10^{-20}$ N m, and apply a steady electric field $E_0 = 10^4$ V m^{-1}. As shown in figure 2, the radius of the bubble hardly changes, so that the compressibility of gas does not play a role and the membrane stress dominates the dynamics of the bubble. The applied electric field does not move the bubble, as shown in the time development of translational velocity in figure 2 and predicted in (2.58). The main effect of the applied electric field is to elongate the bubble. Figure 3(*a*) suggests the second- and fourth-order shape modes develop under the electric field and become stable to be a new shape within 0.2 s. This time scale is close to Kummrow & Helfrich's result. Plotting the shape at the stable state based on the magnitudes of different shape modes and comparing with Kummrow & Helfrich's observation, we find that the shapes agree well with each other (figure 3*b*).

The dynamic equations for the shape modes (2.59) and (2.60) are linear oscillation equations in which the coefficient before a_k is related to the natural frequencies. Therefore, substituting (3.3) into (2.59) or (2.60) and neglecting the time variation of R and viscous effects, we obtain the natural frequencies of the shape modes associated with the bending modulus

$$f_k^{bend} = \frac{1}{2\pi} \sqrt{k(k-1)(k+1)^2(k+2)\frac{G_b}{\rho R_0^5}}. \tag{3.5}$$

Notice that the electric stress includes the terms with a_k, implying the applied electric field will change the natural frequency of the shape mode. Here we take the second-order shape mode as an example and derive its natural frequency, including the effect

https://doi.org/10.1017/jfm.2018.170 Published online by Cambridge University Press

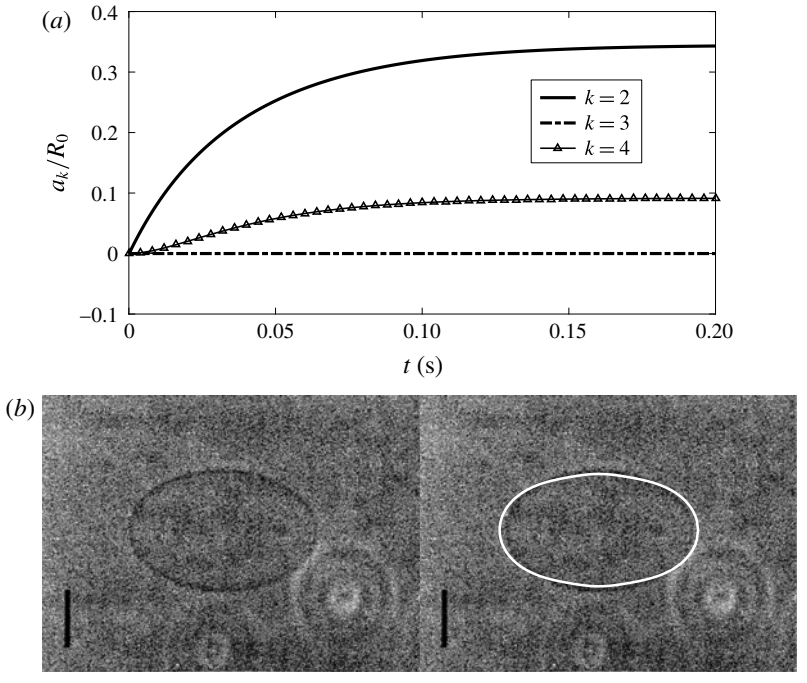


FIGURE 3. (*a*) Time evolutions of shape modes for $k=2$, 3 and 4 for an encapsulated bubble with initial radius $R_0=23$ μm and bending modulus $G_b=2.47\times10^{-20}$ N m under a steady electric field with $E_0=10^4$ V m^{-1}. (*b*) Comparison of the stable shape under $E_0=10^4$ V m^{-1} with the experimental observation by Kummrow & Helfrich (1991). The bar represents 20 μm.

of electric field, as

$$f_2^{ele} = \frac{1}{2\pi}\left[k(k-1)(k+1)^2(k+2)\frac{G_b}{\rho R_0^5} + \frac{6E_0^2}{35\rho R_0}\frac{\varepsilon_0\varepsilon_{ex}(\varepsilon_{ex}-\varepsilon_{in})(52\varepsilon_{ex}^2-109\varepsilon_{ex}\varepsilon_{in}+27\varepsilon_{in}^2)}{(2\varepsilon_{ex}+\varepsilon_{in})^3} + \frac{2q_1E_0}{35\rho R_0}\frac{\varepsilon_{ex}(44\varepsilon_{ex}^2+506\varepsilon_{ex}\varepsilon_{in}-325\varepsilon_{in}^2)}{(2\varepsilon_{ex}+\varepsilon_{in})^3} - \frac{2q_1^2}{35\rho R_0}\frac{128\varepsilon_{ex}^3+772\varepsilon_{ex}^2\varepsilon_{in}+417\varepsilon_{ex}\varepsilon_{in}^2-62\varepsilon_{in}^3}{(2\varepsilon_{ex}+\varepsilon_{in})^3(4\varepsilon_{ex}+3\varepsilon_{in})}\right]^{1/2}, \tag{3.6}$$

where $k=2$. With the parameters adopted in the present work, the modification to the natural frequency due to the electric field is less than 1 %. Hence we can calculate the natural frequency of the shape mode simply by (3.5) to be $f_2^{bend}=2.6$ Hz. Nevertheless, (3.6) indicates that the effect of an electric field on the natural frequency will enhance as its magnitude E_0 increases. In (3.6), the third and fourth terms in square brackets, which are related to q_1, are calculated to be much smaller than the second term, related to E_0^2, according to the results below (see figure 4). The sign of the second term is determined by the sign of $(\varepsilon_{ex}-\varepsilon_{in})$ if ε_{ex} and ε_{in} are significantly different, as in the case of a bubble or a drop. Therefore, the natural frequency

https://doi.org/10.1017/jfm.2018.170 Published online by Cambridge University Press

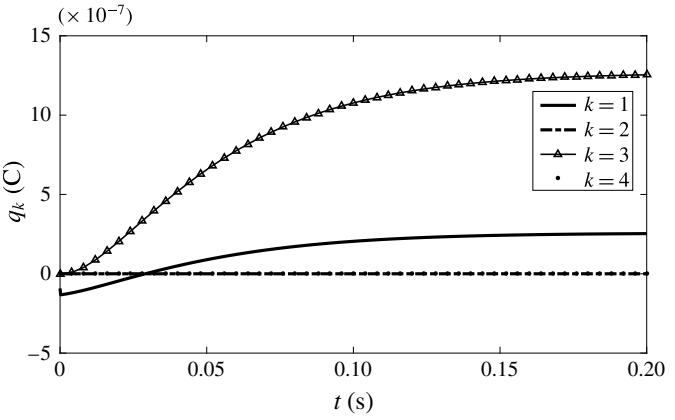


FIGURE 4. Distribution of free charge at the interface versus time for an encapsulated bubble with initial radius $R_0 = 23$ μm and bending modulus $G_b = 2.47 \times 10^{-20}$ N m under a steady electric field with $E_0 = 10^4$ V m^{-1}.

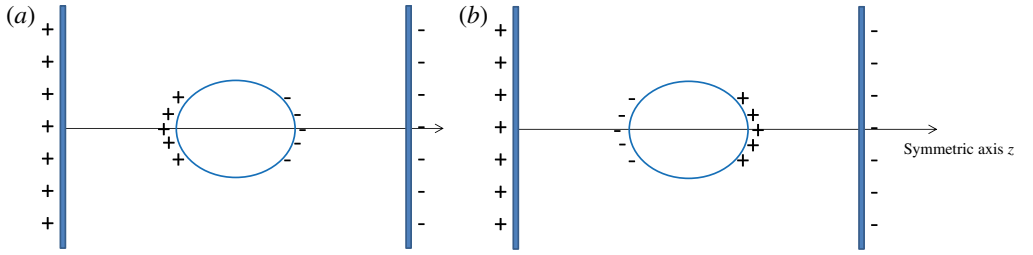


FIGURE 5. (Colour online) Sketch of charge distribution for both (*a*) negative q_1 and (*b*) positive q_1.

increases with increasing electric field for a bubble with $\varepsilon_{ex} > \varepsilon_{in}$, and this trend is opposite for a drop with $\varepsilon_{ex} < \varepsilon_{in}$. These characteristics have been demonstrated by Lee & Kang (1999).

The time evolutions of charge distributions are shown in figure 4. At the beginning, q_1 is negative, which corresponds to the distribution as figure 5(*a*), i.e. the negative charge accumulates at the pole closer to the negative plate electrode while the positive charge is closer to the positive plate electrode. The sign of q_1 transits to be positive as time goes. The transition of the sign can be explained by investigating (2.73). Since the radius does not change (figure 2) and q_2 remains zero (figure 4), the terms including $\dot{R}$ and q_2 are eliminated here. Substituting A_1 (2.13) and B_1 (2.14), (2.73) becomes

$$\dot{q}_1 + \frac{6\dot{a}_2}{5R} q_1 = \frac{3E_0(\varepsilon_{ex}\kappa_{in} - \varepsilon_{in}\kappa_{ex}) - (2\kappa_{ex} + \kappa_{in})\varepsilon_0 q_1}{2\varepsilon_{ex} + \varepsilon_{in}} + \frac{6a_2}{5R} \frac{E_0(\varepsilon_{ex}\kappa_{ex} + 2\varepsilon_{in}\kappa_{ex} - 3\varepsilon_{ex}\kappa_{in}) + q_1\varepsilon_0(\kappa_{ex} + \kappa_{in})}{2\varepsilon_{ex} + \varepsilon_{in}}. \tag{3.7}$$

At the initial time when the charge has not moved and the deformation is not obvious (a_2 is small), the sign of q_1 is determined by the sign of $\varepsilon_{ex}\kappa_{in} - \varepsilon_{in}\kappa_{ex}$. For the present case with gas inside and water outside, $\varepsilon_{ex}\kappa_{in} - \varepsilon_{in}\kappa_{ex} < 0$, so that $q_1 < 0$. As a_2

https://doi.org/10.1017/jfm.2018.170 Published online by Cambridge University Press

increases, the bubble becomes prolate and the second term on the right-hand side of (3.7) dominates the first term, and q_1 becomes positive. Referred to figure 3(*a*), the criterion of a_2/R_0 for the sign transition is approximately 0.19. The value of q_3 is zero at the beginning and develops to be positive with larger magnitude than q_1, since q_3 is induced by a_2 and a_4 according to (2.75), which becomes appreciable as time goes (figure 3*a*). The even order of q_k, such as $k = 2$ and 4, remains zero, as they are induced by the odd order of shape mode, such as a_3, which does not appear in the present case.

3.2. *Membrane with hyperelasticity and bending rigidity*

For a general membrane with hyperelasticity and bending rigidity, we add the hyperelastic stress to the bubble in § 3.1 by setting $G_s = 0.15$ N m^{-1}, which is a moderate elastic modulus for an encapsulated bubble in medical applications (Unnikrishnan & Klibanov 2012), and keeping other parameters unchanged. The time developments of radius, translational velocity, shape modes and charge distributions are shown in figure 6. The time is scaled by the zeroth-order natural frequency calculated by Liu *et al.* (2012) as

$$f_0 = \frac{1}{2\pi}\sqrt{\frac{3\Gamma p_\infty}{\rho R_0^2} + \frac{12G_s}{\rho R_0^3}}. \tag{3.8}$$

Under the resistance from elastic stress, the radius oscillation is at an infinitesimal amplitude and damping due to the liquid viscosity. The translational velocity remains zero. Especially, the deformation of the bubble is much smaller than that of a bubble coated with a bending-resistant membrane. Owing to the small magnitude of shape modes, q_1 becomes stable to a negative value and other mode distribution is not triggered. For a bubble encapsulated by a hyperelastic membrane, a steady electric field has a small effect on its dynamics. As a result, it is not easy to obtain the characteristic parameters such as elastic modulus, natural frequency, etc. using a steady electric field. Even if we increase the electric field, e.g. by applying $E_0 = 10^6$ V m^{-1}, as shown in figure 7, the deformation at the stable state is an order of magnitude smaller than that of the bubble with bending rigidity only (see figure 3*a*).

The results above suggest that the effect of a steady electric field on encapsulated bubble dynamics is small. To explore the effect of a temporally oscillatory electric field, we apply

$$E_0 = E_a \sin(2\pi f_e t), \tag{3.9}$$

where E_a is the amplitude of the oscillatory electric field and f_e is the oscillatory frequency. This electric field is spatially uniform. Similar to the radial mode, the second-order shape mode has a quadratic relation with the electric field E_0 in the dynamic equation (2.59). If we set the electric frequency equal to half of the natural frequency, the shape oscillation is resonant and thus the amplitude of the shape mode is enlarged. The natural frequency of shape modes for the encapsulated bubble is calculated by Liu *et al.* (2012) as

$$f_k^{hp} = \frac{1}{2\pi}\sqrt{2(k-1)(k+1)(k+2)\frac{G_s}{\rho R_0^3}\frac{(2k^2+2k-3)(k^2+k-1+\upsilon)G_b + 6G_sR_0^2}{(k^2+k-1+\upsilon)G_b + 2(2k^2+2k-1)G_sR_0^2}}, \tag{3.10}$$

https://doi.org/10.1017/jfm.2018.170 Published online by Cambridge University Press

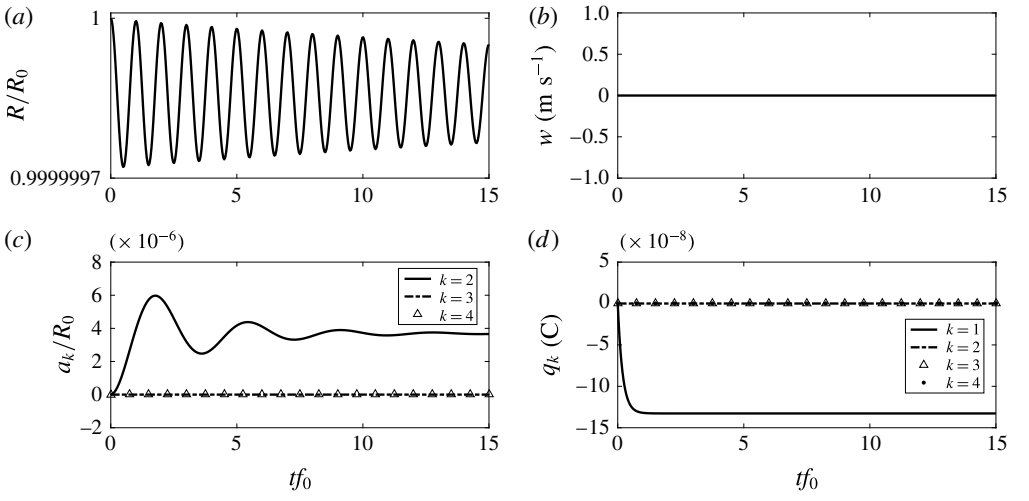


FIGURE 6. Time evolutions of (*a*) radius, (*b*) translational velocity, (*c*) shape modes and (*d*) charge distribution for an encapsulated bubble, with initial radius $R_0 = 23$ μm, elastic modulus $G_s = 0.15$ N m^{-1} and bending modulus $G_b = 2.47 \times 10^{-20}$ N m under a steady electric field with $E_0 = 10^4$ V m^{-1}.

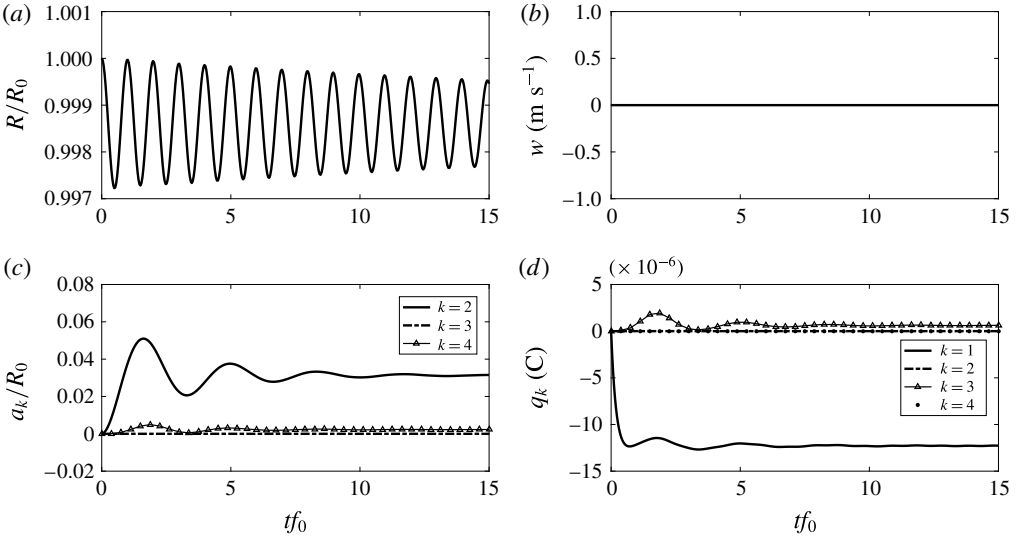


FIGURE 7. Time evolutions of (*a*) radius, (*b*) translational velocity, (*c*) shape modes and (*d*) charge distribution for an encapsulated bubble, with initial radius $R_0 = 23$ μm, elastic modulus $G_s = 0.15$ N m^{-1} and bending modulus $G_b = 2.47 \times 10^{-20}$ N m under a steady electric field with $E_0 = 10^6$ V m^{-1}.

which is $f_2 = 45.2$ kHz for the present bubble. Accordingly, we set $f_e = 22.6$ kHz and find in figure 8 that, although the radius still oscillates at a small amplitude, the second-order shape mode oscillates continuously with an amplitude twofold larger than the stable magnitude under a steady electric field (figure 7*c*). The oscillation of the second-order shape mode reveals the prolate–oblate transition denoted by $a_2 > 0$

https://doi.org/10.1017/jfm.2018.170 Published online by Cambridge University Press

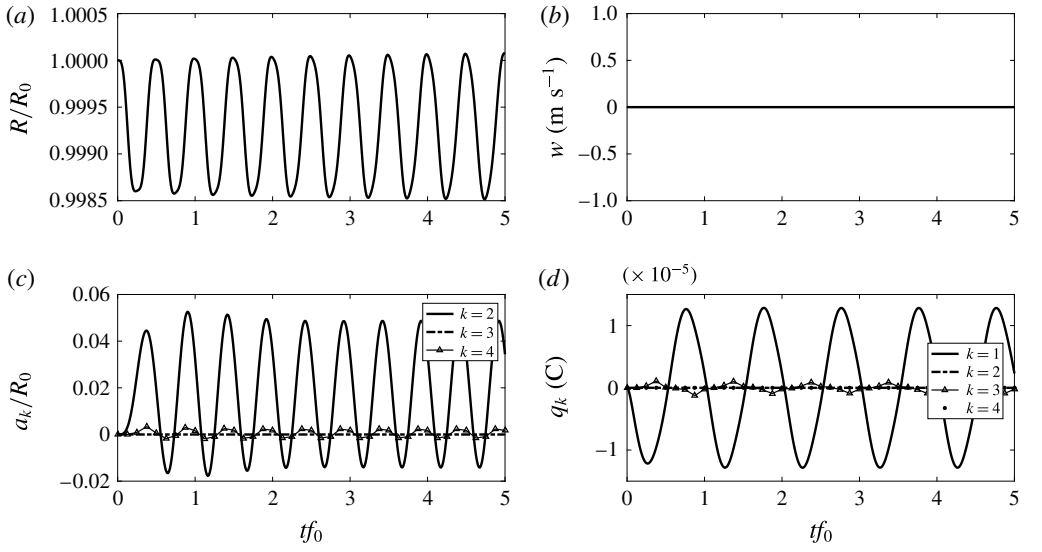


FIGURE 8. Time evolutions of (*a*) radius, (*b*) translational velocity, (*c*) shape modes and (*d*) charge distribution for an encapsulated bubble, with initial radius $R_0 = 23$ μm, elastic modulus $G_s = 0.15$ N m^{-1} and bending modulus $G_b = 2.47 \times 10^{-20}$ N m under an oscillatory electric field with $E_0 = 10^6 \sin(2\pi f_e t)$ V m^{-1}, where $f_e = 22.6$ kHz.

and $a_2 < 0$, respectively. The underlying mechanism is the resonance between the electric frequency and the natural frequency of the shape mode, different from that for a vesicle discussed in Yamamoto *et al.* (2010), for which the prolate–oblate transition is attributed to displacement currents, which redirect the electric fields normal towards the membrane. The displacement currents dominate the conduction currents when the inverse Maxwell–Wagner time $\omega_{MW} = (\kappa_{ex} + \kappa_{in})/[\varepsilon_0(\varepsilon_{ex} + \varepsilon_{in})]$ is lower than the electric frequency. In the present case, ω_{MW} is calculated to be 7×10^5 Hz, higher than the electric frequency we choose, of the order of $O(10^4)$ being the natural frequency of the bubble. This is the reason that we do not include displacement currents in our model.

To obtain the natural frequency of the shape mode for an encapsulated bubble, we can modulate the electric frequency to induce resonance. As an example, we take a gas bubble whose natural frequency of the shape mode has been widely used (Lamb 1932):

$$f_k^{gas} = \frac{1}{2\pi}\sqrt{(k-1)(k+1)(k+2)\frac{\gamma}{\rho R_0^3}}, \tag{3.11}$$

where γ is the coefficient of surface tension, set as 0.0729 N m^{-1} for the gas–water interface. The model in § 2 is applicable by assigning F_n as the surface tension:

$$F_n = \gamma \nabla \cdot \boldsymbol{n} = \frac{2\gamma}{R} + \gamma \sum_{k=2}^{\infty}(k+2)(k-1)\frac{a_k}{R^2}P_k(\cos\theta). \tag{3.12}$$

The interface of a gas bubble is free slip, so that the shear stress $F_t = 0$.

We investigate a gas bubble with the same size as above, $R_0 = 23$ μm, for which the natural frequency of the second-order shape mode is $f_2^{gas} = 42.7$ kHz calculated

https://doi.org/10.1017/jfm.2018.170 Published online by Cambridge University Press

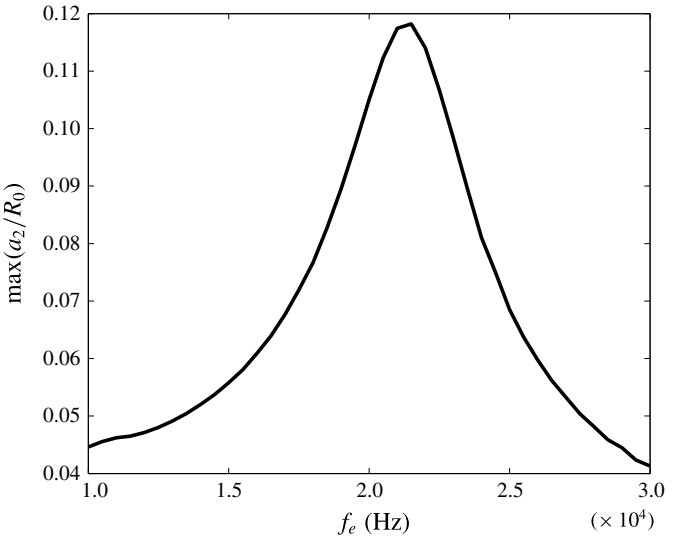


FIGURE 9. The maximal amplitude of the second-order shape mode under various electric field frequencies for a gas bubble with $R_0 = 23$ μm.

by (3.11). Sweeping the electric frequency and recording the maximal amplitude of the second-order shape mode after the transient state, we find that the maximum of amplitude appears at around 21 kHz (figure 9), which is half of its natural frequency. In the same way, we find that the maximum for the encapsulated bubble with $R_0 = 23$ μm, $G_s = 0.15$ N m^{-1} and $G_b = 2.47 \times 10^{-20}$ N m is at approximately 20 kHz (figure 10), slightly less than half of the natural frequency we calculated above ($f_2^{hp}/2 = 22.6$ kHz by (3.10)). The smaller value is attributed to the significant effect of viscosity for an encapsulated bubble, which makes the resonant frequency smaller than the natural frequency without considering the effect of viscosity. Nevertheless, frequency modulation of an oscillatory electric field is a feasible way to estimate the natural frequencies of shape modes. In addition, the maximum a_2 at resonance is more than twice the stable a_2 under a steady electric field, making it easier to detect bubble deformation.

4. Conclusion

In this paper, we have proposed a leaky dielectric model for investigating the dynamics of an encapsulated bubble in an electric field. The applied electric field is spatially uniform and temporally constant or oscillatory. Outside the bubble, we solve a potential flow field with a viscous pressure correction. The electric field and flow field are coupled through force balance on the bubble surface, including electric, hydrodynamic traction and membrane stresses. The system of equations and interface conditions, including the charge transport equation on the bubble surface, are approximated using Legendre polynomials, representing radial, translational and shape oscillations.

Our results for a bubble coated with a bending-resistant membrane show that it undergoes elongated deformation subject to a steady electric field, whose shape agrees well with the observation by Kummrow & Helfrich (1991) with the same parameters. The distribution of charge on the bubble surface is determined by the magnitude of

https://doi.org/10.1017/jfm.2018.170 Published online by Cambridge University Press

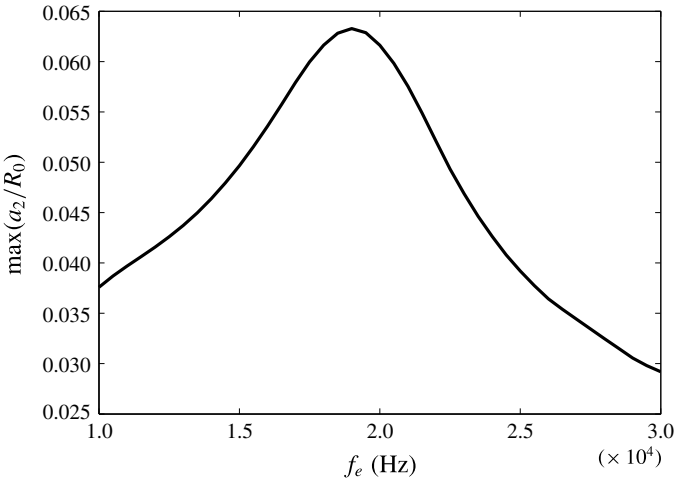


FIGURE 10. The maximal amplitude of the second-order shape mode under various electric field frequencies for an encapsulated bubble with $R_0 = 23$ μm, $G_s = 0.15$ N m^{-1} and $G_b = 2.47 \times 10^{-20}$ N m.

shape modes and the sign of $\varepsilon_{ex}\kappa_{in} - \varepsilon_{in}\kappa_{ex}$. The effect of electric field on the natural frequency is well predicted by our model.

For a hyperelastic membrane with bending rigidity, our results show that the deformation and radial oscillation of an encapsulated bubble are not as visible under a steady applied electric field. By modulating the frequency of an oscillatory electric field, on the other hand, we can induce shape mode resonance. Since the deformation is more significant, natural frequencies of the shape model can be estimated directly with less error.

Acknowledgements

This work was supported by the National Natural Science Foundation of China (11772196, 11372191, 11302128, 11402174), the Natural Science and Engineering Research Council (NSERC) and the Fields Institute of Canada, and the president's fund – research start-up fund from the Chinese University of Hong Kong, Shenzhen.

Appendix A. Relations of the Legendre polynomials

The orthogonal relations of the Legendre polynomials are used throughout this paper. The Legendre polynomials $P_k(\cos\theta)$ and $P_k^1(\cos\theta)$ are simply written as P_k and P_k^1 in this appendix. We have

$$\int_{-1}^{1} P_k P_l \,\mathrm{d}(\cos\theta) = 0, \quad \text{when } k \neq l, \tag{A 1}$$

$$(P_1)^2 = \tfrac{1}{3}(P_0 + 2P_2), \tag{A 2}$$

$$(P_1^1)^2 = \tfrac{2}{3}(P_0 - P_2), \tag{A 3}$$

$$\sum_{k=2}^{\infty} a_k P_1 P_k = \sum_{k=1}^{\infty} \frac{k+1}{2k+3} a_{k+1} P_k + \sum_{k=3}^{\infty} \frac{k}{2k-1} a_{k-1} P_k, \tag{A 4}$$

https://doi.org/10.1017/jfm.2018.170 Published online by Cambridge University Press

$$\sum_{k=2}^{\infty} a_k P_1^1 P_k^1 = \sum_{k=1}^{\infty} \frac{(k+1)(k+2)}{2k+3} a_{k+1} P_k - \sum_{k=3}^{\infty} \frac{k(k-1)}{2k-1} a_{k-1} P_k, \tag{A 5}$$

$$\begin{aligned}\sum_{k=2}^{\infty} a_k P_1 P_1 P_k &= \sum_{k=0}^{\infty} \frac{(k+1)(k+2)}{(2k+3)(2k+5)} a_{k+2} P_k \\ &\quad + \sum_{k=2}^{\infty} \frac{2k^2+2k-1}{(2k-1)(2k+3)} a_k P_k + \sum_{k=4}^{\infty} \frac{k(k-1)}{(2k-3)(2k-1)} a_{k-2} P_k,\end{aligned} \tag{A 6}$$

$$\begin{aligned}\sum_{k=2}^{\infty} a_k P_1 P_1^1 P_k^1 &= \sum_{k=0}^{\infty} \frac{(k+1)(k+2)(k+3)}{(2k+3)(2k+5)} a_{k+2} P_k \\ &\quad + \sum_{k=2}^{\infty} \frac{k(k+1)}{(2k-1)(2k+3)} a_k P_k + \sum_{k=4}^{\infty} \frac{k(k-1)(k-2)}{(2k-3)(2k-1)} a_{k-2} P_k.\end{aligned} \tag{A 7}$$

Appendix B. The interfacial deflection in imposing the boundary condition of an electric field

Based on the axisymmetric coordinate we established, the gradient to the electric potential is written as

$$\nabla \psi = \boldsymbol{e}_r \frac{\partial \psi}{\partial r} + \boldsymbol{e}_\theta \frac{1}{r} \frac{\partial \psi}{\partial \theta}, \tag{B 1}$$

where the subscripts '*ex*' or '*in*' are omitted temporarily for brevity. The projections of electric field to the normal and tangential directions are expressed as

$$\boldsymbol{n} \cdot \nabla \psi = \frac{\partial \psi}{\partial r} - \frac{1}{r^2} \frac{\partial \psi}{\partial \theta} \sum_{k=2}^{\infty} a_k P_k^1, \tag{B 2}$$

$$\boldsymbol{t} \cdot \nabla \psi = \frac{1}{r} \frac{\partial \psi}{\partial r} \sum_{k=2}^{\infty} a_k P_k^1 + \frac{1}{r} \frac{\partial \psi}{\partial \theta}. \tag{B 3}$$

According to the forms of electric potential (2.11) and (2.12), the terms in (B 2) and (B 3) are expanded with respect to the interface deflection defined in (2.1) and (2.2) as follows:

$$\begin{aligned}\frac{\partial \psi_{ex}}{\partial r} &= -\left(E_0 - \frac{2A_1 R^3}{r^3}\right) P_1 + \sum_{k=2}^{\infty} (k+1) \frac{A_k}{r^{k+2}} P_k \\ &= (-E_0 + 2A_1) P_1 - \frac{6A_1}{R} \sum_{k=2}^{\infty} a_k P_1 P_k + \sum_{k=2}^{\infty} (k+1) \frac{A_k}{R^{k+2}} P_k,\end{aligned} \tag{B 4}$$

$$\frac{1}{r} \frac{\partial \psi_{ex}}{\partial \theta} = -(E_0 + A_1) P_1^1 - \sum_{k=2}^{\infty} \frac{A_k}{R^{k+2}} P_k^1, \tag{B 5}$$

$$\frac{\partial \psi_{in}}{\partial r} = -B_1 P_1 - \sum_{k=2}^{\infty} k B_k R^{k-1} P_k, \tag{B 6}$$

$$\frac{1}{r} \frac{\partial \psi_{in}}{\partial \theta} = -B_1 P_1^1 - \sum_{k=2}^{\infty} B_k R^{k-1} P_k^1. \tag{B 7}$$

https://doi.org/10.1017/jfm.2018.170 Published online by Cambridge University Press

Appendix C. Derivation of the right-hand side of (2.69)

We denote the right-hand side of (2.69) as

$$D = \frac{\mathrm{d}q}{\mathrm{d}t} + q\nabla_s \cdot \bar{\boldsymbol{u}} \tag{C 1}$$

and derive its detailed expression in this section.

First, write out the Lagrangian derivative as

$$D = \frac{\partial \widetilde{q}}{\partial t} + (\bar{\boldsymbol{u}} \cdot \nabla)\widetilde{q} + q\nabla_s \cdot \bar{\boldsymbol{u}}, \tag{C 2}$$

where $\widetilde{q}$ is the extension of q to the neighbourhood of the interface, in order to calculate the time derivative and gradient. Decomposing $\bar{\boldsymbol{u}}$ into the tangential and normal components $\bar{\boldsymbol{u}} = \bar{\boldsymbol{u}}_s + \bar{\boldsymbol{u}}_n$ yields

$$D = \frac{\partial \widetilde{q}}{\partial t} + (\bar{\boldsymbol{u}}_n \cdot \nabla)\widetilde{q} + (\bar{\boldsymbol{u}}_s \cdot \nabla)\widetilde{q} + q\nabla_s \cdot \bar{\boldsymbol{u}}. \tag{C 3}$$

By using $\bar{\boldsymbol{u}}_s \cdot \nabla = \bar{\boldsymbol{u}} \cdot \nabla_s$, the above final two terms can be combined and (C 3) is rewritten as

$$D = \frac{\partial \widetilde{q}}{\partial t} + (\bar{\boldsymbol{u}}_n \cdot \nabla)\widetilde{q} + \nabla_s \cdot (q\bar{\boldsymbol{u}}). \tag{C 4}$$

Further decomposing $\bar{\boldsymbol{u}}$ into the tangential and normal components as $\bar{\boldsymbol{u}} = \bar{\boldsymbol{u}}_s + (\bar{\boldsymbol{u}} \cdot \boldsymbol{n})\boldsymbol{n}$,

$$D = \frac{\partial \widetilde{q}}{\partial t} + (\bar{\boldsymbol{u}}_n \cdot \nabla)\widetilde{q} + \nabla_s \cdot (q\bar{\boldsymbol{u}}_s) + q(\nabla_s \cdot \boldsymbol{n})(\bar{\boldsymbol{u}} \cdot \boldsymbol{n}) + (\bar{\boldsymbol{u}} \cdot \boldsymbol{n})\boldsymbol{n} \cdot \nabla_s q, \tag{C 5}$$

the last term of which is zero due to orthogonality, so that D becomes

$$D = \frac{\partial \widetilde{q}}{\partial t} + (\bar{\boldsymbol{u}}_n \cdot \nabla)\widetilde{q} + \nabla_s \cdot (q\bar{\boldsymbol{u}}_s) + q(\nabla_s \cdot \boldsymbol{n})(\bar{\boldsymbol{u}} \cdot \boldsymbol{n}). \tag{C 6}$$

Referring to the method by Pereira *et al.* (2007), who treated surfactant on a horizontal film, we extend their work to the charge on a spherical interface and rewrite (C 6) as

$$D = \frac{\partial q}{\partial t} + \bar{\boldsymbol{u}}_n \cdot \boldsymbol{e}_\theta \frac{1}{r}\frac{\partial q}{\partial \theta} + \nabla_s \cdot (q\bar{\boldsymbol{u}}_s) + q(\nabla_s \cdot \boldsymbol{n})(\bar{\boldsymbol{u}} \cdot \boldsymbol{n}), \tag{C 7}$$

where the time derivative is regarded as at a fixed θ under the assumption that θ and the bubble interface (zero contour of S) are a one-to-one map, which is true in the present case. The derivations to the terms in (C 7) are given below. Here we neglect the coupling effect of a_k and w on the charge transport, i.e. eliminate the terms with $a_k w$. Thus we have

$$\begin{aligned}
\bar{\boldsymbol{u}}_n \cdot \boldsymbol{e}_\theta \frac{1}{r}\frac{\partial q}{\partial \theta} &= (\bar{\boldsymbol{u}} \cdot \boldsymbol{n})\boldsymbol{n} \cdot \boldsymbol{e}_\theta \frac{1}{r}\frac{\partial q}{\partial \theta} \\
&= -\dot{R}\sum_{k=2}^{\infty}\frac{a_k}{R}P_k^1 \sum_{k=1}^{\infty}\frac{1}{R}q_k P_k^1 \\
&= -\frac{\dot{R}q_1}{R^2}\sum_{k=2}^{\infty} a_k P_1^1 P_k^1
\end{aligned}$$

https://doi.org/10.1017/jfm.2018.170 Published online by Cambridge University Press

$$= -\frac{\dot{R}q_1}{R^2}\left[\sum_{k=1}^{\infty}\frac{(k+1)(k+2)}{2k+3}a_{k+1}P_k - \sum_{k=3}^{\infty}\frac{k(k-1)}{2k-1}a_{k-1}P_k\right]$$
$$= P_1\left(-\frac{6}{5}q_1\frac{\dot{R}a_2}{R^2}\right) + P_2\left(-\frac{12}{7}q_1\frac{\dot{R}a_3}{R^2}\right)$$
$$+ \sum_{k=3}^{\infty}P_k\left[-\frac{\dot{R}q_1}{R^2}\left(\frac{(k+1)(k+2)}{2k+3}a_{k+1} - \frac{k(k-1)}{2k-1}a_{k-1}\right)\right], \quad \text{(C 8)}$$

$$\nabla_s\cdot(q\bar{\boldsymbol{u}}_s) = P_1\left[\frac{2}{5}q_1\left(\frac{\dot{a}_2}{R} - \frac{\dot{R}a_2}{R^2}\right) + \frac{2}{5}q_2\left(-\frac{3w}{2R} + \frac{1}{R}\int_R^{\infty}s^{-1}T_1(s,t)\,\mathrm{d}s\right)\right]$$
$$+ P_2\left[q_1\left(\frac{3w}{R} - \frac{2}{R}\int_R^{\infty}s^{-1}T_1(s,t)\,\mathrm{d}s + \frac{6\dot{a}_3}{7R} - \frac{12}{7}\frac{\dot{R}a_3}{R^2}\right)\right.$$
$$\left. + q_3\left(-\frac{9}{7}\frac{w}{R} + \frac{6}{7R}\int_R^{\infty}s^{-1}T_1(s,t)\,\mathrm{d}s\right)\right]$$
$$+ \sum_{k=3}^{\infty}P_k\left\{q_1\left[\frac{k(k+1)}{2k+3}\left(\frac{\dot{a}_{k+1}}{R} - \frac{k\dot{R}a_{k+1}}{R^2}\right)\right.\right.$$
$$\left. + \frac{(k-1)(k+1)}{2k-1}\left(\frac{\dot{a}_{k-1}}{R} - (k-2)\frac{\dot{R}a_{k-1}}{R^2}\right)\right]$$
$$\left. + \left(q_{k+1}\frac{k(k+1)}{2k+3} - q_{k-1}\frac{k(k+1)}{2k-1}\right)\left(-\frac{3w}{2R} + \frac{1}{R}\int_R^{\infty}s^{-1}T_1(s,t)\,\mathrm{d}s\right)\right\}, \quad \text{(C 9)}$$

$$q(\nabla_s\cdot\boldsymbol{n})(\bar{\boldsymbol{u}}\cdot\boldsymbol{n}) = P_1\left[q_1\left(\frac{2\dot{R}}{R} + \frac{8}{5}\frac{a_2\dot{R}}{R^2} + \frac{4}{5}\frac{\dot{a}_2}{R}\right)\right]$$
$$+ P_2\left[q_1\left(\frac{30}{7}\frac{a_3\dot{R}}{R^2} + \frac{6\dot{a}_3}{7R} - \frac{4a_2}{7R^2}\int_R^{\infty}s^{-1}T_1(s,t)\,\mathrm{d}s\right) + q_2\frac{2\dot{R}}{R}\right]$$
$$+ \sum_{k=3}^{\infty}P_k\left\{q_1\left[\frac{k+1}{2k+3}\left(k(k+3)\frac{a_{k+1}\dot{R}}{R^2} + \frac{2\dot{a}_{k+1}}{R}\right)\right.\right.$$
$$+ \frac{k}{2k-1}\left((k+1)(k-2)\frac{a_{k-1}\dot{R}}{R^2} + \frac{2\dot{a}_{k-1}}{R}\right)$$
$$\left. - \frac{2k(k+1)}{(2k-1)(2k+3)}\frac{a_k}{R^2}\int_R^{\infty}s^{-1}T_1(s,t)\,\mathrm{d}s\right] + q_k\frac{2\dot{R}}{R}\left.\right\}. \quad \text{(C 10)}$$

REFERENCES

BARTHÈS-BIESEL, D. & RALLISON, J. M. 1981 The time-dependent deformation of a capsule freely suspended in a linear shear flow. *J. Fluid Mech.* **113**, 251–267.

BATCHELOR, G. K. 2000 *An Introduction to Fluid Dynamics*, chap. 3.1, Cambridge University Press.

BRENNER, M. P., HILGENFELDT, S. & LOHSE, D. 2002 Single-bubble sonoluminescence. *Rev. Mod. Phys.* **74** (2), 425–484.

CHANG, K. & OLBRICHT, W. L. 1993*a* Experimental studies of the deformation and breakup of a synthetic capsule in steady and unsteady simple shear flow. *J. Fluid Mech.* **250**, 609–633.

https://doi.org/10.1017/jfm.2018.170 Published online by Cambridge University Press

CHANG, K. & OLBRICHT, W. L. 1993*b* Experimental studies of the deformation of a synthetic capsule in extensional flow. *J. Fluid Mech.* **250**, 587–608.

CHATTERJEE, D. & SARKAR, K. 2003 A Newtonian rheological model for the interface of microbubble contrast agents. *Ultrasound Med. Biol.* **29** (12), 1749–1757.

CHURCH, C. C. 1995 The effects of an elastic solid surface layer on the radial pulsations of gas bubbles. *J. Acoust. Soc. Am.* **97** (3), 1510–1521.

DE JONG, N., EMMER, M., VAN WAMEL, A. & VERSLUIS, M. 2009 Ultrasonic characterization of ultrasound contrast agents. *Med. Biol. Engng Comput.* **47** (8), 861–873.

DE LOUBENS, C., DESCHAMPS, J., BOEDEC, G. & LEONETTI, M. 2015 Stretching of capsules in an elongation flow, a route to constitutive law. *J. Fluid Mech.* **767**, R3.

DE LOUBENS, C., DESCHAMPS, J., EDWARDS-LEVY, F. & LEONETTI, M. 2016 Tank-treading of microcapsules in shear flow. *J. Fluid Mech.* **789**, 750–767.

DONG, W., LI, R. Y., YU, H. L. & YAN, Y. Y. 2006 An investigation of behaviours of a single bubble in a uniform electric field. *Exp. Therm. Fluid Sci.* **30** (6), 579–586.

DUBASH, N. & MESTEL, A. J. 2007 Behaviour of a conducting drop in a highly viscous fluid subject to an electric field. *J. Fluid Mech.* **581**, 469–493.

FENG, Z. C. & LEAL, L. G. 1997 Nonlinear bubble dynamics. *Annu. Rev. Fluid Mech.* **29** (1), 201–243.

FERRARA, K., POLLARD, R. & BORDEN, M. 2007 Ultrasound microbubble contrast agents: fundamentals and application to gene and drug delivery. *Annu. Rev. Biomed. Engng* **9**, 415–447.

GRACIÀ, R. S., BEZLYEPKINA, N., KNORR, R. L., LIPOWSKY, R. & DIMOVA, R. 2010 Effect of cholesterol on the rigidity of saturated and unsaturated membranes: fluctuation and electrodeformation analysis of giant vesicles. *Soft Matt.* **6** (7), 1472–1482.

GREEN, A. E. & ADKINS, J. E. 1960 *Large Elastic Deformations and Non-Linear Continuum Mechanics*. Clarendon Press.

HELFRICH, W. 1973 Elastic properties of lipid bilayers: theory and possible experiments. *Z. Naturforsch.* C **28** (11–12), 693–703.

KANG, I. S. 1993 Dynamics of a conducting drop in a time-periodic electric field. *J. Fluid Mech.* **257**, 229–264.

KNOCHE, S., VELLA, D., AUMAITRE, E., DEGEN, P., REHAGE, H., CICUTA, P. & KIERFELD, J. 2013 Elastometry of deflated capsules: elastic moduli from shape and wrinkle analysis. *Langmuir* **29** (40), 12463–12471.

KUMMROW, M. & HELFRICH, W. 1991 Deformation of giant lipid vesicles by electric fields. *Phys. Rev.* A **44** (12), 8356.

KWAN, J. J. & BORDEN, M. A. 2012 Lipid monolayer collapse and microbubble stability. *Adv. Colloid. Interface Sci.* **183**, 82–99.

LACOUR, T., GUÉDRA, M., VALIER-BRASIER, T. & COULOUVRAT, F. 2018 A model for acoustic vaporization dynamics of a bubble/droplet system encapsulated within a hyperelastic shell. *J. Acoust. Soc. Am.* **143** (1), 23–37.

LAMB, H. 1932 *Hydrodynamics*. Cambridge University Press.

LANDAU, L. D., LIFSHITZ, E. M. & PITAEVSKII, L. P. 1984 *Electrodynamics of Continuous Media*, 2nd edn. Elsevier Butterworth-Heinemann.

LEE, S. M. & KANG, I. S. 1999 Three-dimensional analysis of the steady-state shape and small-amplitude oscillation of a bubble in uniform and non-uniform electric fields. *J. Fluid Mech.* **384**, 59–91.

LEFEBVRE, Y., LECLERC, E., BARTHÈS-BIESEL, D., WALTER, J. & EDWARDS-LÉVY, F. 2008 Flow of artificial microcapsules in microfluidic channels: a method for determining the elastic properties of the membrane. *Phys. Fluids* **20** (12), 123102.

LINDNER, J. R. 2004 Microbubbles in medical imaging: current applications and future directions. *Nat. Rev. Drug Discov.* **3** (6), 527–533.

LIU, Y., SUGIYAMA, K. & TAKAGI, S. 2016 On the interaction of two encapsulated bubbles in an ultrasound field. *J. Fluid Mech.* **804**, 58–89.

LIU, Y., SUGIYAMA, K., TAKAGI, S. & MATSUMOTO, Y. 2011 Numerical study on the shape oscillation of an encapsulated microbubble in ultrasound field. *Phys. Fluids* **23** (4), 041904.

https://doi.org/10.1017/jfm.2018.170 Published online by Cambridge University Press

LIU, Y., SUGIYAMA, K., TAKAGI, S. & MATSUMOTO, Y. 2012 Surface instability of an encapsulated bubble induced by an ultrasonic pressure wave. *J. Fluid Mech.* **691**, 315–340.

LOVE, A. E. H. 1888 The small free vibrations and deformation of a thin elastic shell. *Phil. Trans. R. Soc. Lond.* A **179**, 491–546.

MARMOTTANT, P., VAN DER MEER, S., EMMER, M., VERSLUIS, M., DE JONG, N., HILGENFELDT, S. & LOHSE, D. 2005 A model for large amplitude oscillations of coated bubbles accounting for buckling and rupture. *J. Acoust. Soc. Am.* **118** (6), 3499–3505.

VAN DER MEER, S. M., DOLLET, B., VOORMOLEN, M. M., CHIN, C. T., BOUAKAZ, A., DE JONG, N., VERSLUIS, M. & LOHSE, D. 2007 Microbubble spectroscopy of ultrasound contrast agents. *J. Acoust. Soc. Am.* **121** (1), 648–656.

MELCHER, J. R. & TAYLOR, G. I. 1969 Electrohydrodynamics: a review of the role of interfacial shear stresses. *Annu. Rev. Fluid Mech.* **1** (1), 111–146.

MOONEY, M. 1940 A theory of large elastic deformation. *J. Appl. Phys.* **11**, 582–592.

PEREIRA, A., TREVELYAN, P. M. J., THIELE, U. & KALLIADASIS, S. 2007 Dynamics of a horizontal thin liquid film in the presence of reactive surfactants. *Phys. Fluids* **19** (11), 112102.

PLESSET, M. S. & PROSPERETTI, A. 1977 Bubble dynamics and cavitation. *Annu. Rev. Fluid Mech.* **9** (1), 145–185.

POZRIKIDIS, C. 2001 Effect of membrane bending stiffness on the deformation of capsules in simple shear flow. *J. Fluid Mech.* **440**, 269–291.

PROSPERETTI, A. 1977 Viscous effects on perturbed spherical flows. *Q. Appl. Maths* **34** (4), 339–352.

PROSPERETTI, A. 1991 The thermal behaviour of oscillating gas bubbles. *J. Fluid Mech.* **222**, 587–616.

PU, G., BORDEN, M. A. & LONGO, M. L. 2006 Collapse and shedding transitions in binary lipid monolayers coating microbubbles. *Langmuir* **22** (7), 2993–2999.

SALIPANTE, P. F. & VLAHOVSKA, P. M. 2014 Vesicle deformation in dc electric pulses. *Soft Matt.* **10** (19), 3386–3393.

SAVILLE, D. A. 1997 Electrohydrodynamics: the Taylor–Melcher leaky dielectric model. *Annu. Rev. Fluid Mech.* **29** (1), 27–64.

SCHNITZER, O. & YARIV, E. 2015 The Taylor–Melcher leaky dielectric model as a macroscale electrokinetic description. *J. Fluid Mech.* **773**, 1–33.

SCHWALBE, J. T., VLAHOVSKA, P. M. & MIKSIS, M. J. 2011 Vesicle electrohydrodynamics. *Phys. Rev.* E **83** (4), 046309.

SEGERS, T., DE ROND, L., DE JONG, N., BORDEN, M. & VERSLUIS, M. 2016 Stability of monodisperse phospholipid-coated microbubbles formed by flow-focusing at high production rates. *Langmuir* **32** (16), 3937–3944.

SHAW, S. J., SPELT, P. D. M. & MATAR, O. K. 2009 Electrically induced bubble deformation, translation and collapse. *J. Engng Maths* **65** (4), 291–310.

SPELT, P. D. M. & MATAR, O. K. 2006 Collapse of a bubble in an electric field. *Phys. Rev.* E **74** (4), 046309.

STONE, H. A. 1990 A simple derivation of the time-dependent convective-diffusion equation for surfactant transport along a deforming interface. *Phys. Fluids* A **2** (1), 111–112.

STRIDE, E. & SAFFARI, N. 2003 On the destruction of microbubble ultrasound contrast agents. *Ultrasound Med. Biol.* **29** (4), 563–573.

STRIDE, E. P. & COUSSIOS, C. C. 2010 Cavitation and contrast: the use of bubbles in ultrasound imaging and therapy. *Proc. Inst. Mech. Engng* H **224** (2), 171–191.

TAYLOR, G. 1964 Disintegration of water drops in an electric field. *Proc. R. Soc. Lond.* A **280**, 383–397.

TRINH, E. H., HOLT, R. G. & THIESSEN, D. B. 1996 The dynamics of ultrasonically levitated drops in an electric field. *Phys. Fluids* **8** (1), 43–61.

TSIGLIFIS, K. & PELEKASIS, N. A. 2008 Nonlinear radial oscillations of encapsulated microbubbles subject to ultrasound: the effect of membrane constitutive law. *J. Acoust. Soc. Am.* **123** (6), 4059–4070.

https://doi.org/10.1017/jfm.2018.170 Published online by Cambridge University Press

TSUKADA, T., KATAYAMA, T., ITO, Y. & HOZAWA, M. 1993 Theoretical and experimental studies of circulations inside and outside a deformed drop under a uniform electric field. *J. Chem. Engng Jpn.* **26** (6), 698–703.

TU, J., GUAN, J., QIU, Y. & MATULA, T. J. 2009 Estimating the shell parameters of SonoVue® microbubbles using light scattering. *J. Acoust. Soc. Am.* **126** (6), 2954–2962.

UNGER, E. C., HERSH, E., VANNAN, M., MATSUNAGA, T. O. & MCCREERY, T. 2001 Local drug and gene delivery through microbubbles. *Prog. Cardiovasc. Dis.* **44** (1), 45–54.

UNNIKRISHNAN, S. & KLIBANOV, A. L. 2012 Microbubbles as ultrasound contrast agents for molecular imaging: preparation and application. *Am. J. Roentgenol.* **199** (2), 292–299.

VAN VLIET, K. J., BAO, G. & SURESH, S. 2003 The biomechanics toolbox: experimental approaches for living cells and biomolecules. *Acta Mater.* **51** (19), 5881–5905.

VIZIKA, O. & SAVILLE, D. A. 1992 The electrohydrodynamic deformation of drops suspended in liquids in steady and oscillatory electric fields. *J. Fluid Mech.* **239**, 1–21.

VLAHOVSKA, P. M., GRACIA, R. S., ARANDA-ESPINOZA, S. & DIMOVA, R. 2009 Electrohydrodynamic model of vesicle deformation in alternating electric fields. *Biophys. J.* **96** (12), 4789–4803.

YAMAMOTO, T., ARANDA-ESPINOZA, S., DIMOVA, R. & LIPOWSKY, R. 2010 Stability of spherical vesicles in electric fields. *Langmuir* **26** (14), 12390–12407.

https://doi.org/10.1017/jfm.2018.170 Published online by Cambridge University Press